博士論文

論文題目　Two-photon fluorescence lifetime imaging of primed SNARE complexes in presynaptic terminals and beta cells

(シナプス前終末と膵 β 細胞におけるSNARE複合体状態の2 光子 FRET 蛍光寿命イメージング)

氏名　　澤田　和可子

TABLE OF CONTENTS

Abstract

It remains unclear how readiness for Ca^{2+}-dependent exocytosis depends on varying degrees of SNARE complex assembly. Here I directly investigate the SNARE assembly using two-photon fluorescence lifetime imaging (FLIM) of Förster resonance energy transfer (FRET) between three pairs of neuronal SNAREs in presynaptic boutons and pancreatic β cells in the islets of Langerhans. These FRET probes functionally rescue their endogenous counterparts, supporting ultrafast exocytosis. I show that *trans*-SNARE complexes accumulated in the active zone, and estimate the number of complexes associated with each docked vesicle. In contrast, SNAREs were unassembled in resting state, and assembled only shortly prior to insulin exocytosis, which proceeds slowly. I thus demonstrate that distinct states of fusion readiness are associated with SNARE complex formation. My FRET/FLIM approaches enable optical imaging of fusion readiness in both live and chemically fixed tissues.

Introduction

Ca^{2+}-dependent exocytosis utilizes soluble *N*-ethylmaleimide- sensitive factor (NSF)-attachment protein receptors (SNAREs) for membrane fusion[1]. Three types of neuronal SNARE proteins—synaptosomal-associated protein 25 (SNAP25) and Syntaxin1A (Syx) in the plasma membrane (t-SNAREs) and vesicle-associated membrane protein 2 (VAMP2) in the vesicle membrane (v-SNARE)—assemble into α-helical four-helix bundles via their SNARE motifs through a zippering process that induces membrane fusion. It has been proposed that SNAREs partially assemble to form *trans*-SNARE complexes that connect the vesicle and plasma membranes and that Ca^{2+} triggers the completion of the zippering reaction, inducing exocytosis via Ca^{2+} sensors termed synaptotagmins and causing the formation of *cis*-SNARE complexes in the plasma membrane[1,2].

This *trans*-SNARE mechanism is particularly suited to ultrafast exocytosis of synaptic vesicles in the active zone (AZ) of presynaptic terminals, where exocytosis is induced within a fraction of millisecond after increases in the cytosolic Ca^{2+} concentration[3]. No study, however, has ever succeeded in demonstrating the *trans*-SNARE complexes in AZ, because quantification of the assembly of the three proteins distinguishing their *trans*- and *cis*-states has been difficult in live cells[4,5].

The *trans*-SNARE complex may not be formed before stimulation[6] in the slow secretory cells[5,7], whereas the *trans*- SNARE mechanism is still assumed in these cells[8,9]. It has thus been largely conjectural how the kinetic diversity of exocytosis depends on the states of SNARE assembly in living cells.

I therefore established Förster resonance energy transfer (FRET) measurements between three pairs of SNARE proteins using t-SNAREs as FRET donors.
I utilized two-photon fluorescence lifetime imaging (FLIM) and the time-correlated single photon counting method to monitor FRET[10,11]. FLIM utilizes only the donor fluorescence, and can estimate inter-molecular FRET, differentiating the FRET efficiency and the binding fraction of two proteins, unlike ratiometric FRET measurement[8,12,13]. SNAREs are the most abundant proteins in presynaptic boutons[14], and are suitable for carrying out FRET analyses with least perturbation of endogenous proteins. I here confirmed that my green fluorescent protein-fused FRET proteins for SNAREs could replace endogenous proteins for ultrafast exocytosis using SNAP25 knockout mice. I established two independent (subtraction and gradient) methods to evaluate the fractions of *trans*-SNARE complexes in the presynaptic boutons of dissociated cultured cortical neurons. I applied the gradient method to hippocampal slice preparations, and found that *trans*-SNAREs were condensed in the AZ apposing

dendritic spines. Moreover, the number of *trans*-SNAREs associated with each docked vesicle in AZ was estimated using the volume of dendritic spine as a proxy for AZ size[15]. In a striking contrast, *trans*-SNAREs were absent in the resting state, and formed only after stimulation in the plasma membrane of β cells in the pancreatic islets of Langerhans, which undergo slow exocytosis of insulin (＞ 1s)[12,16,17]. Thus, I have established an approach to image fusion readiness in various secretory preparations.

Methods

Ethical considerations.

The use and care of animals in this study followed the guidelines of the Animal Experimental Committee of the Faculty of Medicine at the University of Tokyo.

Construction of expression vectors.

Complementary DNAs (cDNAs) of mouse SNAP25b, rat Syx and VAMP2 were kindly provided by Dr. T. Abe, and monomeric Turquoise (mtq) and Venus were provided by Dr. J. Goedhart and Dr. A. Miyawaki, respectively. Mammalian expression vectors for SNAREs were constructed using the ECFP－C1 or －N1 vectors (Clontech Laboratories, Inc., Mountain View, CA, USA), where fluorescence protein was replaced with mtq or Venus, and the promoter was switched from chicken-Beta-Actin (CMV) to cytomegalovirus (CAG).

To construct the N terminal fluorescent probes mtq－SNAP25 and Venus－SNAP25, SNAP25b was amplified with primers 5’-GGCGAATTCAATGGCCGAGGACGCAG-3’and 5’-CCTGTCGACTTAACCACTTCCCAGC-3’and inserted into the EcoRI/SalI site in the multi-cloning site of the C1 vector. To construct the double-fluorescent probe

mtq－Venus－SNAP25, Venus was amplified with the primers

5’-GCCAGATCTATGGTGAGCAAGGGCGAG-3’ and

5’-GGC GAATTCGCCTTGTACAGCTCGTCCATGC-3’ and inserted into the BglII/EcoRI sites of mtq－SNAP25 in the C1 vector. To construct the N terminal fluorescent probes mtq－Syx or Venus－Syx, Syx was amplified with the primers

5’-GCAAGCTT ATGAAGGACCGAACCCAGG-3’ and

5’-CGGTCGACATTCCAAAGATGCCC CCG-3’ and inserted into the Hind III/Sal I site of the C1 vector. To construct the N terminal fluorescent probes Venus－VAMP2 or mVenus－VAMP2, VAMP2 was ampli fied with the primers

5’-GCAAGCTTGTGGTGGTTCTGGTGGTACTGGTGGTTCTGGTAT GTCGGCTACCGCTGC-3’ and

5’-CGCGGATCCCTAAGTGCTGAAGTAAACGATG-3’ and inserted into the HindIII/BamHI sites of the Venus- or monomeric Venus (mVenus)-containing C1 vector. Tetanus toxin (TeNT)－resistant VAMP2 (Q76V, F77W)[61] was prepared with mutagenesis QuikChange II XL system, using primers

5’-CCT CCAGGCAGGGGCCTCCGTGTGGGAAACAAGTGCAGCCAAGC-3’ and

5’-GCTTGGCTGCACTTGTTTCCCACACGGAGGCCCCTGCCTGGAGG-3’.

To construct the C terminal fluorescent probe Syx－Venus, Syx was amplified with

the primers 5’-GGCAAGCTTAT*CGCCACC*ATGAAGGACCGAACCCAGG-3’ and 5’-CGCGTCGACATTCCAAAGATGCCC-3’ and inserted into the HindIII/ SalI sites of the N1 vector (italic sequence means Kozak (Koz) sequence). To construct the C terminal fluorescent probes VAMP2－Venus, VAMP2 was ampli fied with the primers 5’-GCCGCTAGC*CGCCACC*ATGTCGGCTACCGCTGCC-3’ and 5’-CGCGTCGACAGTGCTGAAGTAAACGATGATGAT-3’, and Venus was amplified with the primers 5’-GGGGTCGACGGAGGATCAGGAGGATCAGGA GGAACAGGAAT GGTGAGCAAGGGCGAGG-3’ and 5’-CGCGGATCCTTACTTGTACAGCTCGTCCATGC-3’ and the two digested PCR products were inserted into the NheI/BamHI sites of the N1 vector. CDNAs for the light chain of BoNTE, 51T52N53P, BoNTCα-51 (BoNTC) and TeNT were kindly provided by Dr. H. Gaisano, Dr. M. Jackson and Dr. T. Abe, respectively. I constructed pCAG－Koz－BoNTE－LC－C1 by PCR amplification of the toxin with the primers 5’-GCCGGATCC*CGCCACC*ATGCCAAAAATTAATAGTTTTAATTATAATGATCCT GTTAATG-3’ and 5’-GCCCCCGGGTTACCTTATGCCTTTTACAGAAACAATATTTTTACAAAATCTA ATG-3’ and its insertion into the NheI/SmaI sites of the C1 vector by blunting. pCAG－Koz－BoNTC(51T,52N,53P)－LC－C1 was constructed by PCR amplification of the

toxin with the primers 5'-GCCGCTAGC*CGCCACC*ATGCCAATAACAATTAAC AACTTTAATTATTCAGATCCTG-3' and 5'-GCCGAATTCCTATTTATTATATAATGATCTACCATCTATTGCTTTATGACAAAA TTTTGTAAATA AATAAAGC-3' and its insertion into the NheI/EcoRI sites of the C1 vector. pcDNA3-Koz-TeNT-LC was constructed by PCR amplification of the toxin with the primers 5'-GGCGAATTC*CGCCACC*ATGCCGATCACCATCAACAACT TCC-3' and 5'-CTTGCGGCCGCTTAAGCGGTACGGTTGTACAGG-3' and its insertion into the EcoRI/NotI sites of the C1 vector. All cDNA constructs were confirmed by DNA sequencing.

Dissociated cultured cortical neurons.

Neocortical neurons were dissociated from male Sprague-Dawley rat brains (E19) or C57BL/6 mouse brains (E17.5) with 0.15 % trypsin in 1 % ethylenediaminetetraacetic acid (Invitrogen, Carlsbad, CA, USA) and DNase I (30 μg ml^{-1}). The cells were plated on Laminin- and poly-D-lysine coated cover glasses at a density of 1.7×10^5 cells per cm^2. The neurons were maintained in a serum-free medium (Neurobasal Medium; Invitrogen) supplemented with 500 μM glutamine (rat) or 1 % GlutaMax (mouse) and 2 % B-27 Supplement (Invitrogen). Plasmids for the FRET probes and light-chain

clostridial toxins were transfected by lipofection with Lipofectamine 2000 (Invitrogen; 0.25 %) according to the manufacturer's protocol at 10–12 days after culture, and the cells were observed 1–2 days after lipofection with 0.8–1.2 μg DNA. The standard external bathing solution (SolA) contained 150 mM NaCl, 5 mM KCl, 1 mM $MgCl_2$, 2 mM $CaCl_2$, 10 mM 4-(2-hydroxyethyl)-1-piperazineethanesulfonic acid-NaOH (pH 7.4) and 10 mM glucose for neurons or 2.8 mM glucose for islets (300–310 mOsm). The sucrose solution for stimulating presynaptic terminals contained 300 mM sucrose, and its osmolarity was 610 $mOsml^{-1}$. SNAP25 KO mice were kindly provided from Wilson MC, Takahashi M, Yamamori S. Genotype was de fined by PCR using cerebellar DNA and PrimeSTAR system (TaKaRa Bio). Primer mixtures were NEO588-Forward primer (5'-GCCGAATATCATGGTGGAAA-3'), 25KO-57849FL (5'-CCCACATCTGCCTCCTTTCTGGTT-3') and 25KO-58090RL (5'-GGGATGGGCACCATCAAATCTTTTC-3', 20 μM each). 240 bp band was detected with WT, while 530 bp band was detected with hetero or KO. Lentivirus carrying mtq－SNAP25 and Venus－VAMP2 (TeNT-resistant) was prepared[62], and their promoter regions were substituted into CaMKII promoter. Lentivirus carrying mtq－SNAP25 ($1–3 \times 10^{11}$ genome copies per μl) was transfected in the first day of culture to rescue survival, and lentivirus carrying Venus－VAMP2

(TeNT- resistant) was transfected 2 days before electrophysiological experiments. TeNT- (Lubio Science, 50 ng ml^{-1}) was added 24–36 h before experiments. Tetrodotoxin (TTX) (Wako, Osaka, Japan,10 μM) was added 1–4 h before recordings.

Electrophysiological experiments.

The postsynaptic cells (DIV 12–16) were whole-cell clamped (holding potential = -70mV) and perfused with intracellular solution (in mM: CsCl 140, HEPES 10, MgATP 4, Na_2GTP 0.3, Na_2-phophocreatine 10, Alexa594 0.025, pH = 7.25 with CsOH). Theta-burst stimulation was applied (20 Hz×20 pulse, 100 μA amplitude, 0.1 ms duration, 100–150 μm from dendrites) with 1 or 10 s interval. Extracellular solution was based on SolA containing 10 mM $CaCl_2$, 100 μM cyclothiazide, 50 μM picrotoxin, 320 nM Na-pyruvate and pH 7.4.

Experiments with hippocampal slices.

For slice-cultured neurons, the expression vector was prepared by inserting double-floxed inverted-orientation (DIO) mtq2－Syx, Syx－mtq2, Venus－VAMP2 or VAMP2－Venus into the pAAV vector under the control of the human Syn (hSyn) promoter. The mtq2[32] cDNA was acquired from pCAG－mTq－C1 plasmid by

mutagenesis. Briefly, an I146F mutation was introduced by PCR with primers (5'-AACTACTTTAGCGACAACGTCTAT ATC-3', 5'-GTCGCTAAAGTAGTTGTACTCCAGCTT-3') using PrimeSTAR Max mutagenesis kit (Takara, Japan). The product was digested by Nhe I and BsrG I and was subcloned to the AAV vector. Recombinant AAV1 vectors were produced using previously described methods[63]. In brief, the expression vectors were transfected into AAV293 cells with pHelper (Stratagene, La Jolla, CA, USA) and pRep-Cap AAV1 (Applied Viromics LLC, Fremont, CA, USA) and the cell lysate was purified by CsCl gradient, dialysed and concentrated using Amicon Ultra filters (EMD Millipore, Billerica, MA, USA).

Viral titre was determined by quantitative reverse transcription (qRT)–PCR using primers designed to detect the promoter regions. Hippocampal slices (350 μm thick) were prepared at P7 from SD rat, mounted on 0.4 μm culture plate inserts (EMD Millipore) and incubated at 35 ℃ in an atmosphere of 5 % CO_2 in medium comprising 50 % minimum essential medium (Invitrogen), 25 % Hanks' balanced salt solution (Invitrogen), 25 % horse serum (Invitrogen) and 6.5 gl^{-1} glucose.

AAV mixture (for example, AAV－hSyn－DIO－mTq2－Syx1A, AAV－hSyn－DIO－Venus－VAMP2 and cre expression vector; AAV1. CAMKII 0.4 Cre.SV40 (Penn Vector Core, Philadelphia, PA USA)) was injected into CA3 pyramidal cell layer

at P8–9, using glass micropipette (diameter ~ 6 μm). The mixture also contained 0.03 % Fast Green. Transfection of pCAG－mCherry was done by Gene gun at P14–19 (3.5 μg per 30 μl gold) to visualize postsynaptic dendrite. In the electrophysiological experiments, slices were individually transferred to recording chambers and superfused with artificial cerebral spinal fluid containing 125 mM NaCl, 2.5 mM KCl, 2 mM $CaCl_2$, 1 mM $MgCl_2$, 1.25 mM NaH_2PO_4, 26 mM $NaHCO_3$, 200 μM Trolox (Sigma-Aldrich Corporation, St Louis, MO, USA), 5 nM TTX and 20 mM glucose bubbled with 95 % O_2 and 5 % CO_2. All physiological experiments were performed at 32–34 ℃.

For the imaging of cellular structures and Ca^{2+} transients evoked by electrical stimulation of presynaptic fibres, neurons were transfected with mCherry and GCaMP6s (Plasmid #40753, Addgene, Cambridge, MA, USA), respectively, using a gene gun (PDS-1000; Bio-Rad Laboratories, Inc., Hercules, CA, USA) at P14 and used for experiments between P17 and P22.

Culture and gene transfer with pancreatic islets.

Pancreatic islets were isolated from male imprinting control region (ICR) mice (＞ 8-weeks old) by collagenase digestion (Sigma-Aldrich Corporation) as described previously[59]. The islets were infected with a lentiviral vector carrying cDNA of the

fluorescent probes for 24–72 h in Dulbecco's modified Eagle's medium (glucose 1 gl^{-1}) supplemented with 10 % foetal bovine serum, 100 Uml^{-1} penicillin and 100 mg ml^{-1} streptomycin[36]. Before imaging, the islets were transferred on to thin (0.1 mm) glass coverslips (Matsunami Glass Ind., Ltd., Osaka, Japan) in the recording chamber.

As for the lentiviral vector system, in brief, cDNAs of fluorescent SNAREs were inserted into the FCMV－WPRE vector, and virus particles were produced by their cotransfection with pCMV－VSV－G and pCMV－dR8.9 into lenti-X cells. The viruses were purified by ultracentrifugation and their titre was checked using an qRT–PCR titration kit (6×10^9 genome copies per ml; Lenti-X; Clontech Laboratories, Inc.).

Immunostaining.

For immunostaining, neurons in dissociated culture and pancreatic islets were washed with phosphate-buffered saline (PBS), fixed with 4 % paraformaldehyde for 1 h (4 ℃), washed with PBS, permeabilized with 0.3 % Triton X-100 for 5 h and blocked with 2.5 % horse serum and 0.15 % Triton X-100 for 8 h. The primary antibodies, anti-SNAP25 polyclonal antibody (SNAP25 specific and unable to bind SNAP23; immunogen: 195–206 AA; ab5666; Abcam, Cambridge, UK; 1:100), anti-VAMP2

rabbit polyclonal antibody (VAMP2-specific and unable to bind VAMP1, 3, 4 and 8; immunogen: 1–18 AA; ab3347; Abcam; 1:1000), anti-Syx antibody (also possibly binds Syx1B; ab41453; 1:200) and anti-synaptophysin antibody (MAB5258; EMD Millipore; 1:200), were applied for 8 h, following which the samples were washed with PBS and the secondary antibody was applied (Alexa-Fluor 594-labelled goat anti-mouse Immunoglobulin G (H+L); Invitrogen; 1:800) for 8 h. After a final wash, the preparations immersed in PBS were observed using two-photon microscopy. Fluorescence intensities of Alexa-Fluor 594 were quantified in many plasma membrane regions in the pancreatic islets or in the presynaptic terminal regions of neurons. The intrinsic expression of SNAREs was measured by Alexa-Fluor 594 intensity after secondary antibody labelling. The expression levels of mtq－or Venus－labelled SNAREs were compared with endogenous expression, taking into account the reduction in the fluorescent intensity of mtq and Venus resulting from fixation to 50.2 % and 31 %, respectively.

Two-photon excitation FLIM.

Two-photon excitation imaging was performed using an inverted laser-scanning microscope (FV1000 and IX81; Olympus Corporation, Tokyo, Japan) equipped with a

water-immersion objective lens (UPlanApo60xW/IR; numerical aperture 1.2; Olympus Corporation) and a femtosecond laser (Mai Tai; Spectra Physics Inc., Mountain View, CA, USA) for dissociated culture and β cells in the islets. For slice experiments, an upright microscope (BX61WI; Olympus Corporation) with a LUMPlanFL60xW objective (numerical aperture 0.9; Olympus Corporation) was used. Fluorescence of Alexa-Fluor 594, Venus and mtq was excited at 830 nm and detected at 570–650 nm, 515–560 nm and 460–500 nm, respectively. The autofluorescence was ＞ 2 % of mtq fluorescence in my expression levels, and could not contribute to the lifetime measurement. To measure Venus intensity, the excitation wavelength was set at 970 nm. I confirmed that a spectral bleed through of Venus into the mtq channel was undetectable in my expression levels irrespective of the excitation wavelength of 830 or 970 nm even after repeated imaging sessions. Laser power was set at 4.5 mW. Pixel size was 0.10 μm and 512×512 pixels, with a frame rate of 1 frame per 6 s. For the acceptor bleaching experiment, dissociated culture preparations were irradiated with a Hg lamp at wavelength of 500–550 nm for about 40 min. FLIM of dissociated culture and β cells in the islets was performed using a GaAsP avalanche-diode hybrid detector (R10467U-40; Hamamatsu Photonics K. K., Hamamatsu, Japan) and analysed using SPCImage software (SPC-150; Becker & Hickl GmbH, Berlin, Germany).

For hippocampal slice preparations, I used GaAsP PMT (H7422; Hamamatsu Photonics K. K.) and analysed data using PicoHarp (PicoQuanta GmbH, Berlin) and homemade MATLAB software (MathWorks, Inc., Natick, MA, USA). The fluorescence decay time course fitted a double-exponential function, with time constants of 0.5 and 3.5 ns for mtq, which were convoluted with a Gaussian system response function with a s.d. of 0.1 ns. A faster decay component (A1) values were not critically dependent on the fast time constant between 0.5 and 1 ns. The fast time constant was well-predicted by the short linkers between SNAREs and mtq (or Venus) of 18–25 amino acids in my constructs with predicted lengths of 2.3–2.7 nm, assuming that the length of flexible linker was estimated as 0.86 nm per 2.4 amino acids[64], and that the physical length depends on the square root of the number of amino acids[65,66]. Comparable lengths of linkers were used for FRET/FLIM probes, and resulted in similar fast lifetime decays in other studies[26,67]. Because the fluorescence decay of mtq was 3.5 ns (τ_2) and it did not decay completely within the 12.5 ns sampling interval (T), Ai obtained from doubleexponential fitting was multiplied by ($1-e^{-T/\tau i}$), and then normalized by $A_1+A_2 = 1$ (incomplete multi-exponential fitting)[68]. This process is simple, and the usage of fluorescent probe with a slow fluorescent lifetime decay is beneficial for a better separation of the fast FRET component. The A1 fractions were pseudocolour coded, and

the luminosities of the colour code were modulated on the basis of the brightness of mtq. In the time-lapse experiments, each image of A1 was calculated with a detection time of 20 s and filtered by a median filter with a size of 2 × 2 pixels. In the time-lapse experiments, the A1 fractions were obtained in two different ways. One way was the curve fitting of the average of data from many boutons. The other way was to use the average lifetime to calculate A1, assuming that τ_1 and τ_2 were constantly 0.5 and 3.5 ns and using the equations $(T_{ave} - T_0) = \frac{A1\,\tau1^2 + A2\,\tau2^2}{A1\,\tau1 + A2\,\tau2}$ and $A_1 + A_2 = 1$, where T_{ave} is the average lifetime and T_0 is the offset arrival time, obtained by fitting the fluorescence of a large region-of-interest[10]. To measure mtq and mCherry in hippocampal slice preparations, the excitation wavelength was set at 900 nm and fluorescence was detected at 460–500 nm and 570–650 nm, respectively. Laser power was set at 5–8 mW. Pixel size was 0.079 μm (128 × 128 pixels). Three-dimensional FLIM images were obtained by 20 s imaging for each depth with 1 μm interval (seven depths).

The Venus images were acquired at 520–560 nm at 980 nm excitation wavelength, and Z-stacks had an interval of 1 μm with a frame rate of 1 frame per 0.8 s.

I estimated spine-head volume (V) from the total fluorescence intensity (F) in the stacked images of spines. A conversion coefficient, V/F, was obtained from the fluorescence profile of the largest, roundest spine on each dendrite[69,70], which was

subsequently applied to all other spines on the dendrite. For Ca^{2+} imaging, two-photon excitation was performed at 970 nm and the fluorescence intensity of GCaMP6s was measured at 490–540 nm. The signals were obtained from all spines. Pixel size was 0.1 μm, and images were acquired at a rate of 1 frame per 0.22 s. Two-photon images were analysed using IPLab (Scanalytics Inc., Milwaukee, WI, USA), ImageJ (the National Institutes of Health, Bethesda, MD, USA; http://rsb.info.nih.gov/ij/) and MATLAB software. Detection of insulin exocytic events was performed as described in a previous paper[12]. Shortly, I immersed the pancreatic islets expressing the FRET probes with SolA containing 0.3 mM Alexa594 hydrazide (Invitrogen), and stimulated insulin secretion with 16 mM glucose and 5 nM GLP-1. The individual exocytic events were captured with 2P imaging by the sudden appearance of small fluorescent spots inside the islet[16]. I simultaneously performed time-lapsed measurements of Alexa 594 intensity at 570–650 nm (Fluoview) and FLIM of mtq at 460–500 nm with an interval of 1.8 s. I used excitation wavelength of 830 nm, and the power of 4–5 mW. Exocytic events detected within 40 min were analysed.

Statistical analysis.

The FRET images which did not have sufficient photon counts were discarded from

statistical analysis. Comparable numbers of images were used as in previous studies[8,12,13]. Histogram bars represent the mean ± s.e.m. The significance of each A1 fraction versus 0 % was tested using the Wilcoxon signed-rank test. The differences between two groups were tested using the Mann–Whitney *U*-test.

For multiple comparisons between groups, the significance was first examined using the Kruskal–Wallis test, followed by Scheffé's or Steel's tests. The significances of the correlation coefficient were tested using Spearman's rank correlation coefficient. No randomization and blinding was used to analyse the data.

Results

Estimation of binding fractions of SNAREs with FRET/FLIM.

To quantify assembly between the three pairs of SNARE proteins, I labelled the t-SNAREs SNAP25b and Syx with mtq to form FRET donors and VAMP2 and Syx with the FRET acceptor Venus (Fig. 1a—f and Fig. 2). The constructs were lipofected into cortical neurons in dissociated culture. Images were acquired for 60 s to accumulate a sufficient number of photons for constructing fluorescence lifetime curves.

The fluorescence lifetime of mtq－SNAP25b (Fig. 1g—i) was monoexponential, with a time constant of ~3.5 ns, in synaptic boutons (Fig. 1 h,i; A2), indicating that mtq is an appropriate probe for quantitative FLIM[18,19]. The A1, with time constants of 0.7 ns (τ_1), was evident when both mtq and Venus were fused with SNAP25b in tandem (Fig. 1j—l; A1[20]). The A1was obtained by double-exponential fitting of photon count decays by fixing the slow component as 3.5 ns (τ_2; Methods). The A1 fraction was estimated to be 63.5 % (Fig. 1m) instead of 100 % that would be expected for a tandem probe. This is in line with a previous study[10], and is explained by incomplete maturation or a dark state of Venus. This factor was left uncorrected to avoid possible overestimation of molecular interactions[10].

The values of τ_1 for all the probes (Figs. 1—23) were estimated in between 0.5 and

1.5 ns, indicating that FRET efficiency (= 1-τ_1/τ_2) was between 0.85 and 0.57 and that distances between the two fluorescent proteins in the binding state were within the Förster radius, and therefore the A1 value was used as an estimate of the binding fraction (%) of a SNARE pair. I first analysed FRET probes in neurons in dissociated culture and then applied them to intact synapses in slice preparations, as I am using two-photon imaging, then compared the results with those of β cells in the islets of Langerhans.

Syx-based FRET probes in synaptic boutons.

The time constant of the fluorescence decay of mtq－Syx was monoexponential and unaffected by chemical fixation (Fig. 3a—d). I confirmed that Syx-positive boutons were presynaptic structures by counterstaining mtq－Syx preparations with anti-synaptophysin antibody (Fig. 3c). There was no gradient of A1 values within a single bouton around the synaptophysin-positive spots (Fig. 3c; A1). However, significant A1 fractions appeared within a bouton (Fig. 4a,b) when Venus－VAMP2 was cotransfected with mtq－Syx. I confirmed that the A1 fraction represented FRET, because it was eliminated by bleaching of Venus (Fig. 4c,d). Comparable A1 fractions were obtained when I used the monomerizing A206K mutant of mVenus (Fig. 4e,f),

in which dimerization of Venus and binding between mtq and Venus were minimized[21].The A1 values did not seem to depend on expression levels of the donor mtq－Syx, but correlated with the expression of the acceptor Venus－VAMP2 (Fig. 5a,b). Endogenous expression of Syx and VAMP2 were estimated using an antibody against Syx and VAMP2 as 80 A.U. and 540 A.U., respectively (Fig. 5c,d; Methods), where the specificity of the antibodies to VAMP2 was confirmed by transfecting the light chains of TeNT, which selectively cleaves VAMP2, and removed 90 % of antigenicity (Fig. 6a,b). The A1 fraction was 34.1 % in boutons when expression levels of VAMP2 were similar to endogenous levels (Fig. 5b). This A1 fraction should predict the binding fraction of endogenous Syx with VAMP2, given that the FRET signal showed an approximately linear increase with VAMP2 expression levels (Fig. 5b). The A1 fraction was not ascribed to molecular crowding of SNAREs in AZ because the homotypic binding between mtq－Syx and Venus－Syx (Fig. 7a—f), and between mtq －SNAP25 and Venus－SNAP25 (Fig. 7g—m), were negligible at all expression levels, whereas all three heteromeric pairs of SNAREs (Syx/VAMP2, SNAP25/VAMP2 and SNAP25/Syx) showed significant binding (Fig. 8a—c; see Fig. 13e and Fig. 14e).

Chemical fixation did not affect fluorescence lifetimes[22] and FRET values (Fig. 8a—c), and I found that synaptophysin-positive sites in boutons showed FRET in

the A1 fraction of 38.8 %, whereas the synaptophysin-negative parts showed FRET in the A1 fraction of 17.4 % (Fig. 8d; see Fig. 18j—l for more precise arrangement of vesicles and the high FRET region). This suggests that the Syx- and VAMP2-binding fractions were larger in the AZ. In contrast, the A1 fraction was only ~ 22 % in axons on average (Fig. 8d). These binding fractions included both *trans*- and *cis*-SNARE complexes.

To quantify *cis*-SNARE complex separately from *trans*-complex[1], I labelled SNAREs at their C-termini so that FRET occurred only for *cis*-SNARE complexes (Fig. 9a). A1 values were estimated to be 24.7 % at the endogenous level of VAMP2 expression (Fig. 9b—g). Since the total fraction of SNARE complexes was estimated as 34.1 % (Fig. 8c), this provided an estimate of the fraction of Syx that forms *trans*-SNARE complexes with VAMP2 of 9.4 % (= 34.1-24.7) on average (Table 1; subtraction method). Unlike the A1 fractions of total SNARE complexes (Fig. 8c), those of *cis*-SNAREs were similar between boutons and axons (Fig. 9g; 24.7 versus 21.5 %). Moreover, the A1 fractions in the boutons (A1bouton) were similar to those in the axons (A1axon) surrounding each bouton (Fig. 9h), suggesting that *cis*-SNAREs are diffusible and equilibrate along axons. Furthermore, *cis*-complex was nearly eliminated by lipofection of the light chain of botulinum toxin, BoNTE,

which selectively cleaves SNAP25 and blocks exocytosis (Fig. 9g and Fig. 10a,b)[23,24], suggesting that *cis*-SNARE complexes form at boutons by exocytosis and diffuse into axons.

To test whether *trans*-SNARE complexes are converted into *cis*-SNARE complexes by exocytosis, I stimulated the boutons with a hypertonic sucrose solution, which is known to induce the exocytosis of vesicles in the readily releasable pool[25]. I found that *cis*-SNARE complexes formed in the boutons as the decay lifetime shortened there (Fig. 10c), suggesting that *cis*-SNARE complexes form from *trans*-SNARE complexes by exocytosis[1]. For time-resolved analysis, I accumulated images for 18 s from several boutons to which sucrose was applied. I therefore estimated the A1 fraction from both fitting of decay time courses and the average lifetime (T_{A1bouton}; open circles), assuming a τ_1 of 0.5 ns (Methods)[26]. Increases in the A1 fraction were consistently estimated by the two methods (mean ± s.e. of seven experiments: 11.8 ± 1.7 and 12.9 ± 3.7 % ; Fig. 10d). This value was similar with the fraction of *trans*-SNARE complexes of 10 % estimated by the subtraction method (and the gradient method, see below), suggesting that all *trans*-SNARE complexes were converted into *cis*-SNARE complexes after exocytosis. Consistent with this observation, the sucrose-induced increases in A1 values were abrogated by BoNTE treatment (Fig. 10e). These data support that

trans-SNAREs in the boutons identified by FRET of mtq－Syx/Venus－VAMP2 actually represented the ternary complexes, and prepared for exocytosis. The A1 fractions also increased in axons after sucrose stimulation (Fig. 10c,d, T_{A1axon}), confirming the diffusion of *cis*-SNAREs into axons[13].

Transfection of neurons with BoNTE reduced (but did not eliminate) the A1 fraction of the mtq－Syx/Venus－VAMP2 probe from 34.1 to 16.3 % in boutons (Fig. 11 a—c). The remaining complexes may be *trans*-SNAREs, because BoNTE nearly eliminated *cis*-SNARE (Fig. 9g), possibly by blockade of exocytosis (Fig. 10a). In fact, the BoNTE-resistant fraction (16.3 %) was close to the *trans*-complex fraction estimated with the subtraction method. It is surprising that the *trans*-complex can be formed to a similar degree even without SNAP25 (Fig. 11c), suggesting that AZ helps assemble the binary complex.

The SNARE complexes in axons are unlikely to be *trans*-complexes because vesicles are not docked in the axon. In fact, the amount of total SNARE complexes present in axons (Fig. 11b,c; 22.4 %) was similar to that of *cis*-SNARE complexes (Fig. 9g; 21.5 %) in axons. Because the fractions of *cis*-SNARE were similar between axons and boutons (Fig. 9g,h; 24.7 %), the fraction of *trans*-SNARE complexes in boutons can be calculated by the difference between the SNARE complexes in boutons

and axons as 11.7 % (= 34.1-22.4; Table 1; gradient method) similar with the value (9.4 %) obtained by the subtraction method. The gradient method could be applied to each bouton because the fraction of SNARE complexes in each bouton (A1bouton) was linearly related to that of the axon surrounding the bouton (Fig. 11d, A1axon) and subtraction of A1axon from A1bouton yielded the fraction of *trans*-SNARE in each bouton as 11.6 ± 1.0 % (n = 36; Fig. 11e), independently of the A1axon values. The sizes of boutons showed only a weak correlation with the *trans*-SNARE fractions (Fig. 11f), indicating that the sizes of boutons are not a good indicator of presynaptic function[27], unless the sizes of AZs were taken into account (see Fig. 18n). I also found that TTX reduced SNARE complexes along axons within 1h (Fig. 12a), indicating that *cis*-SNAREs in the axons were dependent on neuronal activity, consistent with the results with BoNTE (Fig. 9g). Importantly, however, the amount of *trans*-SNARE complexes in the boutons estimated by the gradient method was unaltered up to 4 h (Fig. 12b). This indicated that the abundant *trans*-SNAREs in the boutons were assembled in the absence of action potentials, and supported the *trans*-SNARE model for ultrafast exocytosis[5].

SNAP25-based FRET probes in synaptic boutons.

I examined whether the fraction of *trans*-SNARE complexes obtained by

SNAP25-based FRET probes was similar (Fig. 13a,b). The A1 fraction was 36.7 % in the boutons when expression levels of VAMP2 were similar for the endogenous level on average (Fig. 5d and Fig. 13c—e). The difference between the SNARE complexes in boutons and the surrounding axons estimated *trans*-SNARE to be 14.0 % (= 36.7-22.7) in a bouton (Table 1). This value was similar to those obtained using Syx-based probes (11.7 %, Table 1), suggesting that the expression levels of SNAP25 and Syx were similar in boutons. Indeed, the endogenous expression of SNAP25 and Syx was estimated to be 98 A.U. and 80 A.U., respectively, using mtq probes in boutons (Fig. 5c and Fig. 9f), as in the whole brain preparation[14]. The specificity of the antibodies to Syx and SNAP25 was confirmed by transfecting the light chains of BoNTC1α-51 which selectively cleaves Syx[28] and BoNTE (Fig. 6b and Fig. 13f,g). The fraction of *trans*-SNAREs was also estimated using mtq－SNAP25b and Venus－Syx (Fig. 14a—e). The A1 fraction was 29.5 % in boutons and 16.2 % in axons for the endogenous expression level of Syx (Fig. 7f and Fig. 14e), predicting that 13.3 % (= 29.5-16.2) exists as *trans*-SNARE complexes (Table 1).

The A1 fractions in the boutons were reduced to 14.5 % and 12.0 % by BoNTC1α-51 (Fig. 13e) and TeNT (Fig. 14e—g)[24], respectively. It was again noted that SNAP25/VAMP2 and SNAP25/Syx binary complexes remained in boutons, even

though those in axons were eliminated (Fig. 14e—g). The fractions were similar with the estimated SNARE complex fractions of 14.0 % and 13.3 % (Table 1), respectively, as in the case with BoNTE (Fig.11c and Fig. 13e), suggesting the existence of efficient mechanisms to assemble the binary complexes in AZ.

To confirm that the FRET probes did not affect the dynamics of exocytosis and refilling of vesicles, I examined excitatory postsynaptic currents (EPSCs) evoked by electrical stimulation in the presence of cyclothiazide, which prevents the desensitization of AMPA receptors (Fig. 15a)[29], and studied the time courses of ultrafast exocytosis, depletion and refilling of glutamatergic vesicles in wild-type (WT) mice by repetitive stimulation at 20 Hz 20 times (Fig. 15b—g). SNAP25 was replaced with mtq－SNAP25 using knockout mice[30] where synaptic transmission was abolished (Fig. 15h,i), and rescued by mtq－SNAP25 (Fig. 15j,k). VAMP2 was then cleaved by TeNT treatment, and rescued by TeNT-resistant VAMP2 (VAMP (TeNTR)) fused with Venus (Fig. 15l—q). In this preparation, I found the same ultrafast exocytosis as in the WT (Fig. 15a,n). EPSCs occurred with delays of about 2.5 ms, and the time to peak was 0.4ms in the WT, SNAP25 KO with mtq－SNAP25 and SNAP25 KO with mtq-SNAP25/Venus－VAMP (TeNTR) in the presence of TeNT. Thus, the kinetics of exocytosis was unaffected. Furthermore, ultrafast exocytosis was depleted within

20 times of stimulation (Fig. 15o). This depletion lasted for at least 1s (Fig. 15o,q), and recovered over a 10-s interval as in the WT (Fig. 15e).

Thus, the depletion and refilling of vesicles were unaffected by replacing endogenous proteins with mtq－SNAP25/Venus－VAMP2. The FRET levels were similarly estimated as 24.4 % in boutons and 13.1 % in axons (Fig. 16a,b and Table 1), predicting *trans*-SNAREs to be about 11.3 % of the SNARE population, where the average expression levels of mtq－SNAP25 and Venus－VAMP2 were similar to endogenous levels (Fig. 5d and Fig. 9f). I therefore conclude that my SNARE FRET/FLIM probes can measure the functional states of SNAREs without affecting the dynamics of SNAREs.

Imaging of presynaptic SNARE complexes in slice cultures.

I next applied my two-photon FRET/FLIM probes to the CA1 region of hippocampal slice cultures, where postsynaptic spines can be identified and the sizes of AZ can be estimated from the size of spines[15,26,31]. Fluorescence decay of mtq2－Syx[32] was monoexponential with a time constant of 3.8ns in the Schaffer collaterals in the CA1 region (Fig. 17). I first confirmed whether the *trans*-complex fraction was similar in the slice preparation by sucrose. To express the Syx－mtq2/VAMP2－Venus probes in

Schaffer collateral fibres in the CA1 region, AAV1 vectors were injected into the CA3 region (Fig. 18a,b). FRET of *cis*-complexes between Syx－mtq2 and VAMP2－Venus was 3.7 ± 1.2 % (n = 24) in the resting state, and the A1 fraction was increased to 13.6 % ± 1.8 % (n = 24) during sucrose stimulation (Fig. 18c,d). The fractions of *cis*-SNARE in the resting state were similar between boutons and axons (Fig. 18e) as seen in dissociated cultures (Fig. 9h), supporting the idea that *cis*-SNAREs diffuse into axons in slice preparations (Fig. 18c), as in dissociated culture.

To measure the distribution of *trans*-SNARE complexes, I expressed mtq2－Syx/Venus－VAMP2 probes in Schaffer collateral fibres using an AAV1 (Fig. 18f), and a gene gun was used to express a plasmid containing mCherry in CA1 pyramidal neurons to visualize dendritic spines. I identified possible contacts between mtq2－positive boutons and mCherry－positive spines by three-dimensional inspection (Fig. 18g,h), where a single laser beam (900 nm) was used so that the position of two images was completely identical. I found that, in cases where presynaptic boutons overlapped with spines (Fig. 18i), mtq2－Syx showed high FRET values in the overlapping region, potentially representing AZ (Fig. 18j). Such overlaps should reflect the interdigited nature of spine synapses[33]. In fact, I also found VAMP2 clusters in such presynaptic boutons (Fig. 18k). When I analysed the fluorescent profiles along the spine

(Fig. 18l), the high FRET regions were closer to the spines than to the presynaptic profiles labelled with VAMP2 or Syx, consistent with the localization of the AZ at the edge of presynaptic vesicle cluster[34]. In my expression level, mCherry fluorescence was not detectable in the mtq channel, and could not be a reason for the high FRET region at the border of boutons.

The fractions of *trans*-SNARE both in boutons on average and within AZ were estimated in the presynaptic boutons, which displayed a clear overlap with a dendritic spine (Fig. 18i). The *trans*-SNARE values were estimated by subtracting the A1 values in the axons surrounding the bouton (A1axon) from those of all boutons (Fig. 18m; A1bouton-A1axon), indicating that the average FRET values in the boutons showed a correlation with spine volume with the mean *trans*-SNARE fraction of 11.9 % (Table 1), reflecting that AZ sizes showed strong correlation with spine volumes[15]. To estimate the *trans*-SNARE fraction within AZ, I used the area of boutons overlapping with spines, and obtained the peak values (A1s) in the images which were smoothed to render the FWHM spatial resolution to 0.5 μm. The peak values of *trans*-SNARE fractions for AZ were correlated with volumes in small spines (Fig. 18n), possibly because of the limited spatial resolution, and because the fraction of *trans*-SNAREs was constant irrespective of AZ size. In fact, the peak values were independent of spine volumes for those spines

$>$ 0.2 μm^3 (Fig. 18n), where corresponding AZ had an area $>$ 0.2 μm^2 and a diameter $>$ 0.5 μm so that the peak value was not attenuated by the limited spatial resolution[15]. For Fig. 18n, I intentionally selected large spines, as they were relatively infrequent. I estimated the fraction of *trans*-SNAREs in AZ using the spines $>$ 0.25 μm^2 as 27.7 % (= A1s-A1axon; Table 1).

To examine the presynaptic functions of spine synapses, I expressed a Ca^{2+} indicator probe, GCaMP6s, in CA1 pyramidal neurons using a gene gun for monitoring Ca^{2+} responses in individual spines (Fig. 19a—d) whose presynaptic fibres were stimulated by a glass electrode. The release probabilities of the boutons were estimated by repetitive stimulation (20 – 50 times) of presynaptic fibres at 0.1 Hz, and spine Ca^{2+} increases $>$ 3 s.d. of the noise level (100 % changes in GCaMP6s) within 0.3 s of stimulation were considered as successful transmission. I found that the spine size strongly correlated with the release probabilities of presynaptic terminals (Fig. 19e), possibly owing to their correlations with the sizes of AZ[35] and the amount of *trans*-SNARE (Fig. 18n).

SNARE complexes in β cells in the islets of Langerhans.

Finally, I examined SNARE complexes in β cells in the islets of Langerhans (Fig. 20a), which I transfected with SNARE probes by lentivirus (Fig. 20b)[36]. I chose cells with

discrete membrane staining inside the islets (Fig. 20a, arrow); 80 % were β cells undergoing insulin secretion[12,16]. When the islets were transfected with mtq－SNAP25b and Venus－Syx (Fig. 20b), a significant A1 fraction appeared in the plasma membrane (Fig. 20c—f). The A1 value was estimated to be 5.3 % at the endogenous expression level of Venus－Syx (Fig. 21a—d). The existence of SNARE complexes in the islets is consistent with a previous study in which the assembly of SNAP25 with Syx was ratiometrically estimated using intramolecular FRET of SNAP25[12]. Using anti-SNARE antibodies and mtq－SNARE probes, I estimated the endogenous levels of SNAP25 and Syx expression to be 92 A.U. and 10 A.U., respectively (Fig. 21c,e). Expression of SNAP25 was nine times greater than that of Syx, as in PC12 cells[37] and may correlate with the small fraction of SNAP25-forming complexes with Syx.

In contrast, binding between t-SNAREs and VAMP2 was not significant (Fig. 20g—l): decay time courses were almost mono-exponential (Fig. 20i,l) when islets were transfected with mtq－Syx or mtq－SNAP25b and Venus－VAMP2 (Fig. 20b). The A1 fractions were ＜ 2 % and were not significantly different from zero for the endogenous expression levels of VAMP2 (Fig. 20f,Fig. 21f and Fig. 22). Thus, no significant *trans*-SNARE complexes exist in the plasma membranes of β cells (Table 1).

To examine whether SNAREs probes reflected functional states in β cells,

I simultaneously imaged individual instances of exocytosis of insulin vesicles with an extracellular tracer, Alexa594 (Fig. 23a,b), and FRET values of mtq－SNAP25b/Venus－VAMP2 for the region with a diameter of 0.5 μm where exocytosis was imaged during islet stimulation by a high-glucose solution (16 mM, Fig. 23c—e). I accumulated fluorescence for 1.8 s, and estimated the A1 fraction from the average lifetime, assuming τ_1 of 0.5 ns as in Fig. 10d. SNAP25b was used instead of Syx, because endogenous expression levels of Syx in β cells were low, and its overexpression was often toxic. I frequently found increases in FRET values before individual exocytotic events (1.8–10.8 s, mean = 5.9 ± 0.3 s, n = 61). The peak value was 8.3 ± 1.6 % in averaged traces from 61 events (Fig. 23f). Such FRET signals were only found in the region surrounding exocytotic events (Fig. 23g). These data suggest that SNAREs are unassembled in the resting state, and they assemble only shortly before exocytosis in β cells (Fig. 23h), unlike synaptic vesicles in boutons where *trans*-SNAREs are already assembled in the resting state for ultrafast exocytosis (Fig. 23i).

Discussion

I have thus succeeded in estimation of *trans*-SNARE fractions of t-SNAREs in neurons and β cells using FRET probes of SNARE proteins. I confirmed that the green fluorescent protein-fused probes could replace the functions of endogenous proteins for ultrafast exocytosis. The *trans*-SNARE fraction was consistently estimated as about 10 % in the entire bouton with various probes, and about 25 % in AZ, while absent from axons and β cells (Table 1). It is of note that the gradient method with VAMP2 can estimate the fraction of *trans*-SNARE in individual boutons. This is based on the finding that most SNARE complexes in the axon were *cis*-SNAREs, and that the fractions of *cis*-SNARE were similar between boutons and their surrounding axons (Fig. 9h and Fig. 18e), possibly because both *cis*-SNARE and free Syx can diffuse along axons, and their proportion is determined by a balance between exocytosis and the actions of NSF[38,39]. I found that the release probability is proportional to sizes of spines, and therefore to AZ sizes and to the fraction of *trans*-SNAREs. My two-photon FRET approaches may be useful for long-term functional imaging of presynaptic terminals whose functional states cannot simply be inferred from their sizes (Fig. 11f)[27], unlike postsynaptic dendritic spines[40]. The fraction of VAMP2-forming complexes with Syx was estimated to be 2–5 % by a previous study of presynaptic boutons[13] in which VAMP2 was used as a

FRET donor. This fraction was small because the FRET signal was diluted by VAMP2 in non-docked vesicles, the major component (90 %) of vesicles in a bouton.

In contrast, I used t-SNARE as FRET donor, and the FRET values are unaffected by non-docked vesicles and report the readiness of exocytosis of the plasma membrane.

I found that ~ 27.7 % of Syx formed *trans*-SNARE complexes in AZ (Fig. 18n).

Recently, the amount of Syx1A was estimated[14] as 20,096 molecules per bouton with an average surface area of 2.31 μm^2. If I assume this value, the number of Syx in AZ per 0.1 μm^2 should be estimated as 870 (= 20,096 × 0.1/2.31), because Syx homogenously distribute in bouton (Fig. 3a and Fig. 18g)[14]. It has been reported that the number of docked vesicles correlates with the area of the AZ, and 25 vesicles are docked per 0.1 μm^2 of AZ[41,42]. By definition, the size of the AZ is nearly the same as the PSD, and the size of the PSD is proportional to the volume of the spine[15], such that a spine with 0.1 μm^2 PSD has 0.1 μm^3 spine volume[15,27,41]. Thus, the number of *trans*-SNAREs associated with each docked vesicle is estimated as 9.6 (= 870 × 0.277/25).

Note all these *trans*-SNAREs may not be used for ultrafast exocytosis. In fact, previous studies suggested the number of functional *trans*-SNAREs required for ultrafast fusion reaction to be in between two and nine[43–46].

The larger *trans*-SNARE fraction in AZ (27 %) than the mean value (10 %) in

bouton reflects the accumulation of docked vesicles in AZ. I demonstrated that AZ promoted assembly of binary SNARE complexes (Syx/SNAP25, Syx/VAMP2, SNAP25/VAMP2) even though one type of the SNARE proteins was cleaved by clostridial toxins, possibly reflecting the fact that docking of synaptic vesicles is often unimpaired by toxin treatment[5]. An AZ protein, Munc13, may contribute in such *trans*-SNARE formation, because it induces Syx open form[47], and its MUN domain can bind free SNARE proteins[48,49]. Alternatively, they may be due to tethering mechanisms, such as those involving voltage-gated calcium channels[50].

I found that the *trans*-SNAREs were accumulated but not exclusively localized in AZ. This is consistent with the observation that docked vesicles are found outside the AZ[42,51], and ectopic exocytosis of synaptic vesicles outside AZ was reported[52–54]. It may also relate to the fact that releasable vesicles are formed close to the Ca^{2+} channels after positional priming[55], and that the most AZ proteins show some condensation in the AZ, but distributed throughout a bouton[14]. Such ectopic *trans*-SNAREs may be utilized for asynchronous exocytosis[56] and tonic exocytosis[57] where increases in $[Ca^{2+}]_i$ spread outside of AZ.

My data indicate that a major fraction of SNARE proteins is unassembled (unitary) outside AZ even in neurons (Table 1)[5], and such unitary SNAREs are predominant in β

cells, where *trans*-SNARE complexes are nearly absent, in line with the fact that insulin vesicles are mostly non-docked to the plasma membrane before exocytosis[5,58]. Indeed, I confirmed the formation of *trans*-SNARE complex shortly preceding slow insulin exocytosis (Fig. 23f)[16,17,59]. Unitary SNAREs may also be utilized in neurons, for example, in slow exocytosis of large dense-core vesicles[60].

In summary, I directly demonstrated an extreme diversity in the initial states of SNARE proteins in synapses and secretory cells, consistent with the marked differences in their readiness for exocytosis. I have thus established the technique to image the readiness for exocytosis in the plasma membrane without actually triggering exocytosis. My two-photon FRET/FLIM methods are widely applicable for functional imaging of presynaptic terminals and secretory cells in both live and fixed preparations[71].

Acknowledgements

This is a reproduced and modified version of an article accepted for publication in Nature Communications 6, Article number:8531(2015):“Two-photon fluorescence lifetime imaging of primed SNARE complexes in presynaptic terminals and β cells. ” Cells.”(reference 71).

I am most grateful to Professor Haruo Kasai and Dr. Noriko Takahashi for their constant support in the course of the present study.

Professor Haruo Kasai and Dr. Noriko Takahashi educated me with tremendous support and guidance and a kindly teaching for my experiments.

I greatly appreciate the advice from Dr. Shigeo Okabe and Dr. Ayako Hayashi at Department of Cellular Neurobiology, Graduate School of Medicine, The University of Tokyo.

I would like to convey my appreciation to Dr. Satoshi Watanabe and Dr. Mituyo Ohno.

I also thank Dr. Hiroshi Tokumaru, Dr. Joachim Goedhart, Dr. Meyer Jackson,

Dr. Herbert Gaisano , Dr. Teruo Abe, Dr. Saori Yamamori, Dr. Masami Takahashi ,Dr. Michael C Wilson , Dr. Jun Noguchi, Dr. Hasan Ucar, Dr. Sho Yagishita, Dr. Akiko Hayashi-Takagi, Dr. Kazuhiko Ishii, Mr. Akira Nagaoka, Dr. Yoshitomo Maeda, Ms. Chiho Maeda, Ms. Mie Ogasawara, Mr. Kazuhito Tamura, Ms. Haruka Ohno, Ms. Masumi Ikeda and Ms. Yasuko Ohki for helpful discussions and valuable supports.

Finally, I would also like to express my gratitude to Takashi Sawada and Kohko Sawada for their endless support and warm encouragements.

References

1. Sudhof TC and Rothman JE (2009) Membrane fusion: grappling with SNARE and SM proteins. Science 323:474-477.

2. Jahn R and Fasshauer D (2012) Molecular machines governing exocytosis of synaptic vesicles. Nature 490:201-207.

3. Lonart G and Sudhof TC (2000) Assembly of SNARE core complexes prior to neurotransmitter release sets the readily releasable pool of synaptic vesicles. J. Biol. Chem. 275:27703-27707.

4. Pang ZP and Sudhof TC (2010) Cell biology of Ca^{2+}-triggered exocytosis. Curr. Opin. Cell Biol. 22:496-505.

5. Kasai H, Takahashi N and Tokumaru H (2012) Distinct initial SNARE configurations underlying the diversity of exocytosis. Physiol. Rev. 92:1915-1964.

6. Chen YA, Scales SJ, Patel SM, Doung YC and Scheller RH (1999) SNARE complex formation is triggered by Ca^{2+} and drives membrane fusion. Cell 97:165-174.

7. Kasai H (1999) Comparative biology of exocytosis: implications of kinetic diversity for secretory function. Trends Neurosci. 22:88-93.

8. Zhao Y, Fang Q, Herbst AD, Berberian KN, Almers W and Lindau M (2013) Rapid structural change in synaptosomal-associated protein 25 (SNAP25) precedes the fusion of single vesicles with the plasma membrane in live chromaffin cells. Proc Natl

Acad Sci U S A 110:14249-54. doi: 10.1073/pnas.1306699110

9. Ashcroft FM and Rorsman P (2012) Diabetes mellitus and the beta cell: the last ten years. Cell 148:1160-71. doi: 10.1016/j.cell.2012.02.010

10. Murakoshi H, Lee SJ and Yasuda R (2008) Highly sensitive and quantitative FRET-FLIM imaging in single dendritic spines using improved non-radiative YFP. Brain Cell Biol. 36:31-42.

11. Rickman C (2010) t-SNARE protein conformations patterned by the lipid microenvironment. J. Biol. Chem. 285:13535-13541.

12. Takahashi N, Hatakeyama H, Okado H, Noguchi J, Ohno M and Kasai H (2010) SNARE conformational changes that prepare vesicles for exocytosis. Cell Metab 12:19-29. doi: 10.1016/j.cmet.2010.05.013

13. Degtyar V, Hafez IM, Bray C and Zucker RS (2013) Dance of the SNAREs: assembly and rearrangements detected with FRET at neuronal synapses. J. Neurosci. 33:5507-5523.

14. Wilhelm BG, Mandad S, Truckenbrodt S, Krohnert K, Schafer C, Rammner B, Koo SJ, Classen GA, Krauss M, Haucke V, Urlaub H and Rizzoli SO (2014) Composition of isolated synaptic boutons reveals the amounts of vesicle trafficking proteins. Science 344:1023-8. doi: 10.1126/science.1252884

15. Harris KM and Stevens JK (1989) Dendritic spines of CA 1 pyramidal cells in the rat hippocampus: serial electron microscopy with reference to their biophysical characteristics. J. Neurosci. 9:2982-2997.

16. Takahashi N, Kishimoto T, Nemoto T, Kadowaki T and Kasai H (2002) Fusion pore dynamics and insulin granule exocytosis in the pancreatic islet. Science 297:1349-1352.

17. Gopel S, Zhang Q, Eliasson L, Ma XS, Galvanovskis J, Kanno T, Salehi A and Rorsman P (2004) Capacitance measurements of exocytosis in mouse pancreatic alpha-, beta- and delta-cells within intact islets of Langerhans. J. Physiol. 556:711-726.

18. Goedhart J, van Weeren L, Hink MA, Vischer NO, Jalink K and Gadella TW, Jr. (2010) Bright cyan fluorescent protein variants identified by fluorescence lifetime screening. Nat. Methods 7:137-139.

19. Walther KA, Papke B, Sinn MB, Michel K and Kinkhabwala A (2011) Precise measurement of protein interacting fractions with fluorescence lifetime imaging microscopy. Mol. Biosyst. 7:322-336.

20. Hink MA, Griep RA, Borst JW, van Hoek A, Eppink MH, Schots A and Visser AJ (2000) Structural dynamics of green fluorescent protein alone and fused with a single chain Fv protein. J Biol Chem 275:17556-60. doi: 10.1074/jbc.M001348200

21. Kotera I, Iwasaki T, Imamura H, Noji H and Nagai T (2010) Reversible dimerization of Aequorea victoria fluorescent proteins increases the dynamic range of FRET-based indicators. ACS Chem. Biol. 5:215-222.

22. Joosen L, Hink MA, Gadella Jr TW and Goedhart J (2014) Effect of fixation procedures on the fluorescence lifetimes of Aequorea victoria derived fluorescent proteins. J. Microscopy 256:166-176.

23. Hayashi T, McMahon H, Yamasaki S, Binz T, Hata Y, Sudhof TC and Niemann H (1994) Synaptic vesicle membrane fusion complex: action of clostridial neurotoxins on assembly. EMBO J. 13:5051-5061.

24. Schiavo G, Matteoli M and Montecucco C (2000) Neurotoxins affecting neuroexocytosis. Physiol. Rev. 80:717-766.

25. Rosenmund C and Stevens CF (1996) Definition of the readily releasable pool of vesicles at hippocampal synapses. Neuron 16:1197-1207.

26. Lee SJ, Escobedo-Lozoya Y, Szatmari EM and Yasuda R (2009) Activation of CaMKII in single dendritic spines during long-term potentiation. Nature 458:299-304.

27. Holderith N, Lorincz A, Katona G, Rozsa B, Kulik A, Watanabe M and Nusser Z (2012) Release probability of hippocampal glutamatergic terminals scales with the size of the active zone. Nat. Neurosci. 15:988-997.

28. Wang D, Zhang Z, Dong M, Sun S, Chapman ER and Jackson MB (2011) Syntaxin requirement for Ca^{2+}-triggered exocytosis in neurons and endocrine cells demonstrated with an engineered neurotoxin. Biochemistry 50:2711-2713.

29. Trussell LO, Zhang S and Raman IM (1993) Desensitization of AMPA receptors upon multiquantal neurotransmitter release. Neuron 10:1185-1196.

30. Washbourne P, Thompson PM, Carta M, Costa ET, Mathews JR, Lopez-Bendito G, Molnar Z, Becher MW, Valenzuela CF, Partridge LD and Wilson MC (2002) Genetic ablation of the t-SNARE SNAP-25 distinguishes mechanisms of neuroexocytosis. Nat. Neurosci. 5:19-26.

31. Matsuzaki M, Honkura N, Ellis-Davies GC and Kasai H (2004) Structural basis of long-term potentiation in single dendritic spines. Nature 429:761-766.

32. Goedhart J, von Stetten D, Noirclerc-Savoye M, Lelimousin M, Joosen L, Hink MA, van Weeren L, Gadella TW, Jr. and Royant A (2012) Structure-guided evolution of cyan fluorescent proteins towards a quantum yield of 93%. Nat. Commun. 3:751.

33. Mishchenko Y, Hu T, Spacek J, Mendenhall J, Harris KM and Chklovskii DB (2010) Ultrastructural analysis of hippocampal neuropil from the connectomics perspective. Neuron 67:1009-1020.

34. Bourne JN, Chirillo MA and Harris KM (2013) Presynaptic ultrastructural

plasticity along CA3-->CA1 axons during long-term potentiation in mature hippocampus. J. Comp. Neurol. 521:3898-3912.

35. Matz J, Gilyan A, Kolar A, McCarvill T and Krueger SR (2010) Rapid structural alterations of the active zone lead to sustained changes in neurotransmitter release. Proc. Natl Acad. Sci. USA 107:8836-8841.

36. Lam PP, Ohno M, Dolai S, He Y, Qin T, Liang T, Zhu D, Kang Y, Liu Y, Kauppi M, Xie L, Wan WC, Bin NR, Sugita S, Olkkonen VM, Takahashi N, Kasai H and Gaisano HY (2013) Munc18b is a major mediator of insulin exocytosis in rat pancreatic beta-cells. Diabetes 62:2416-2428.

37. Knowles MK, Barg S, Wan L, Midorikawa M, Chen X and Almers W (2010) Single secretory granules of live cells recruit syntaxin-1 and synaptosomal associated protein 25 (SNAP-25) in large copy numbers. Proc. Natl Acad. Sci. USA 107:20810-20815.

38. Hohl TM, Parlati F, Wimmer C, Rothman JE, Sollner TH and Engelhardt H (1998) Arrangement of subunits in 20 S particles consisting of NSF, SNAPs, and SNARE complexes. Mol. Cell 2:539-548.

39. Kuner T, Li Y, Gee KR, Bonewald LF and Augustine GJ (2008) Photolysis of a caged peptide reveals rapid action of N-ethylmaleimide sensitive factor before

neurotransmitter release. Proc. Natl Acad. Sci. USA 105:347-352.

40. Noguchi J, Nagaoka A, Watanabe S, Ellis-Davies GC, Kitamura K, Kano M, Matsuzaki M and Kasai H (2011) In vivo two-photon uncaging of glutamate revealing the structure-function relationships of dendritic spines in the neocortex of adult mice. J. Physiol. 589:2447-2457.

41. Schikorski T and Stevens CF (1997) Quantitative ultrastructural analysis of hippocampal excitatory synapses. J. Neurosci. 17:5858-5867.

42. Marra V, Burden JJ, Thorpe JR, Smith IT, Smith SL, Hausser M, Branco T and Staras K (2012) A preferentially segregated recycling vesicle pool of limited size supports neurotransmission in native central synapses. Neuron 76:579-589.

43. Sinha R, Ahmed S, Jahn R and Klingauf J (2011) Two synaptobrevin molecules are sufficient for vesicle fusion in central nervous system synapses. Proc. Natl Acad. Sci. USA 108:14318-14323.

44. Megighian A, Zordan M, Pantano S, Scorzeto M, Rigoni M, Zanini D, Rossetto O and Montecucco C (2013) Evidence for a radial SNARE super-complex mediating neurotransmitter release at the Drosophila neuromuscular junction. J Cell Sci 126:3134-40. doi: 10.1242/jcs.123802

45. Rickman C, Hu K, Carroll J and Davletov B (2005) Self-assembly of SNARE

fusion proteins into star-shaped oligomers. Biochem. J. 388:75-79.

46. Domanska MK, Kiessling V, Stein A, Fasshauer D and Tamm LK (2009) Single vesicle millisecond fusion kinetics reveals number of SNARE complexes optimal for fast SNARE-mediated membrane fusion. J. Biol. Chem. 284:32158-32166.

47. Acuna C, Guo Q, Burre J, Sharma M, Sun J and Sudhof TC (2014) Microsecond dissection of neurotransmitter release: SNARE-complex assembly dictates speed and Ca^{2+} sensitivity. Neuron 82:1088-1100.

48. Khodthong C, Kabachinski G, James DJ and Martin TF (2011) Munc13 homology domain-1 in CAPS/UNC31 mediates SNARE binding required for priming vesicle exocytosis. Cell Metab. 14:254-263.

49. Guan R, Dai H and Rizo J (2008) Binding of the Munc13-1 MUN domain to membrane-anchored SNARE complexes. Biochemistry 47:1474-1481.

50. Wong FK, Nath AR, Chen RH, Gardezi SR, Li Q and Stanley EF (2014) Synaptic vesicle tethering and the CaV2.2 distal C-terminal. Front Cell Neurosci 8:71. doi: 10.3389/fncel.2014.00071

51. Zhou K, Stawicki TM, Goncharov A and Jin Y (2013) Position of UNC-13 in the active zone regulates synaptic vesicle release probability and release kinetics. eLife 2:e01180.

52. Ratnayaka A, Marra V, Branco T and Staras K (2011) Extrasynaptic vesicle recycling in mature hippocampal neurons. Nat. Commun. 2:531.

53. Matsui K and Jahr CE (2003) Ectopic release of synaptic vesicles. Neuron 40:1173-1183.

54. Coggan JS (2005) Evidence for ectopic neurotransmission at a neuronal synapse. Science 309:446-451.

55. Neher E and Sakaba T (2008) Multiple roles of calcium ions in the regulation of neurotransmitter release. Neuron 59:861-872.

56. Raingo J, Khvotchev M, Liu P, Darios F, Li YC, Ramirez DM, Adachi M, Lemieux P, Toth K, Davletov B and Kavalali ET (2012) VAMP4 directs synaptic vesicles to a pool that selectively maintains asynchronous neurotransmission. Nat Neurosci 15:738-45. doi: 10.1038/nn.3067

57. Burgalossi A, Jung S, Meyer G, Jockusch WJ, Jahn O, Taschenberger H, O'Connor VM, Nishiki T, Takahashi M, Brose N and Rhee JS (2010) SNARE protein recycling by alphaSNAP and betaSNAP supports synaptic vesicle priming. Neuron 68:473-87. doi: 10.1016/j.neuron.2010.09.019

58. Hatlapatka K, Matz M, Schumacher K, Baumann K and Rustenbeck I (2011) Bidirectional insulin granule turnover in the submembrane space during K(+)

depolarization-induced secretion. Traffic 12:1166-1178.

59. Takahashi N, Hatakeyama H, Okado H, Miwa A, Kishimoto T, Kojima T, Abe T and Kasai H (2004) Sequential exocytosis of insulin granules is associated with redistribution of SNAP25. J Cell Biol 165:255-62. doi: 10.1083/jcb.200312033

60. van de Bospoort R, Farina M, Schmitz SK, de Jong A, de Wit H, Verhage M and Toonen RF (2012) Munc13 controls the location and efficiency of dense-core vesicle release in neurons. J Cell Biol 199:883-91. doi: 10.1083/jcb.201208024

61. Quetglas S, Iborra C, Sasakawa N, De Haro L, Kumakura K, Sato K, Leveque C and Seagar M (2002) Calmodulin and lipid binding to synaptobrevin regulates calcium-dependent exocytosis. EMBO J 21:3970-9. doi: 10.1093/emboj/cdf404

62. Lois C, Hong EJ, Pease S, Brown EJ and Baltimore D (2002) Germline transmission and tissue-specific expression of transgenes delivered by lentiviral vectors. Science 295:868-872.

63. Gray SJ, Choi VW, Asokan A, Haberman RA, McCown TJ and Samulski RJ (2011) Production of recombinant adeno-associated viral vectors and use in in vitro and in vivo administration. Curr Protoc Neurosci Chapter 4:Unit 4 17. doi: 10.1002/0471142301.ns0417s57

64. Mori MX, Erickson MG and Yue DT (2004) Functional stoichiometry and local

enrichment of calmodulin interacting with Ca^{2+} channels. Science 304:432-435.

65. Cantor CR and Schimmel PR (1980) The Behavior of Biological Macromolecules (Freeman, San Francisco.

66. Evers TH, van Dongen EM, Faesen AC, Meijer EW and Merkx M (2006) Quantitative understanding of the energy transfer between fluorescent proteins connected via flexible peptide linkers. Biochemistry 45:13183-13192.

67. Yasuda R, Harvey CD, Zhong H, Sobczyk A, van Aelst L and Svoboda K (2006) Supersensitive Ras activation in dendrites and spines revealed by two-photon fluorescence lifetime imaging. Nat Neurosci 9:283-91. doi: 10.1038/nn1635

68. Leung RW, Yeh SC and Fang Q (2011) Effects of incomplete decay in fluorescence lifetime estimation. Biomed. Opt. Express 2:2517-2531.

69. Noguchi J, Matsuzaki M, Ellis-Davies GCR and Kasai H (2005) Spine-neck geometry determines NMDA receptor-dependent Ca^{2+} signaling in dendrites. Neuron 46:609-622.

70. Yasumatsu N, Matsuzaki M, Miyazaki T, Noguchi J and Kasai H (2008) Principles of long-term dynamics of dendritic spines. J. Neurosci. 28:13592-13608.

71. Takahashi N, Sawada W, Noguchi J, Watanabe S, Ucar H, Hayashi-Takagi A, Yagishita S, Ohno M, Tokumaru H and Kasai H (2015) Two-photon fluorescence

lifetime imaging of primed SNARE complexes in presynaptic terminals and β cells. Nature Commun 6, Article number:8531

Figures and Figure legends

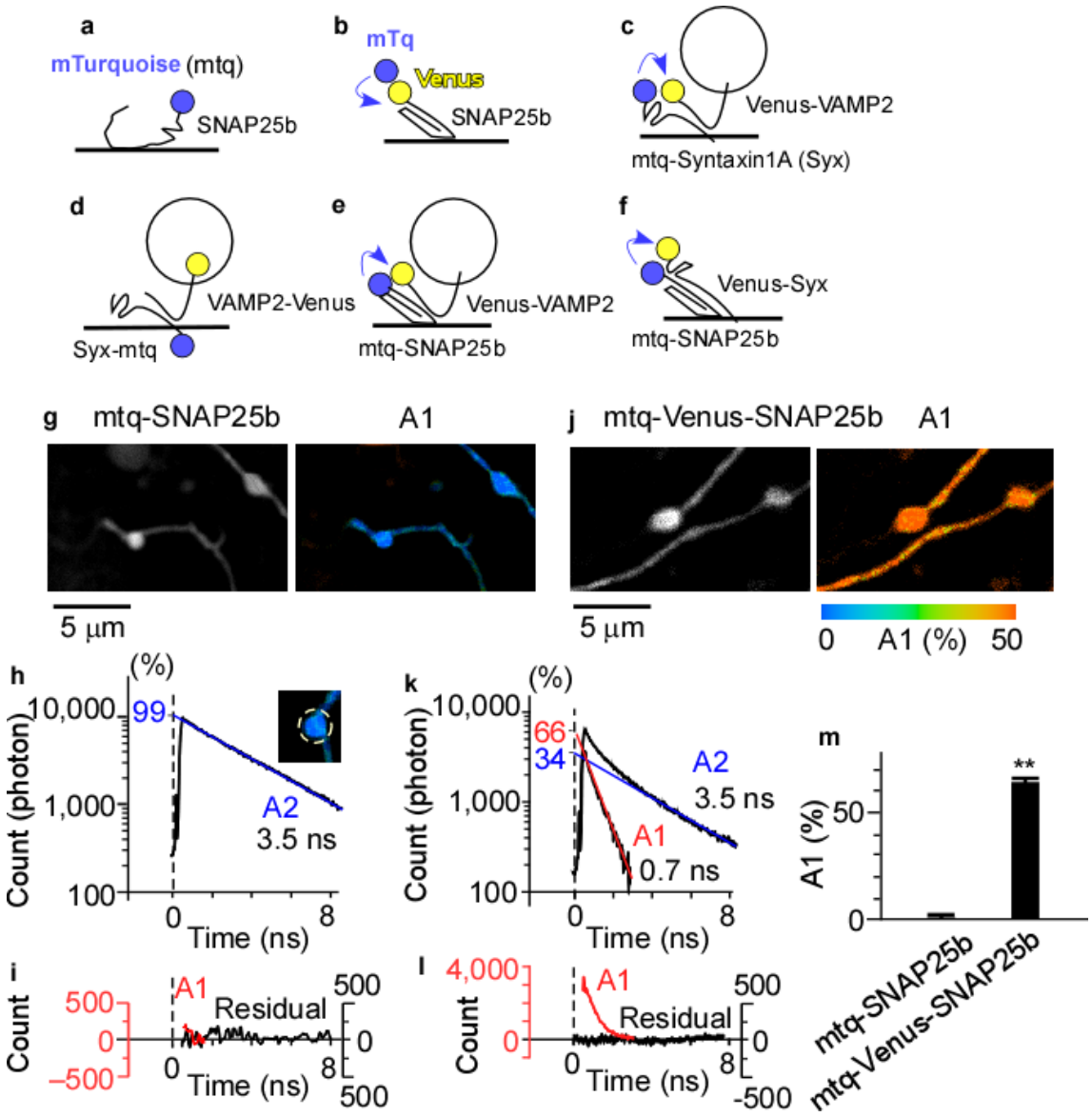

Figure 1 | Combinations of FRET/2pFLIM probes for SNAREs.

(a—f) Schematic drawing of combinations of probes whose constructs are depicted in Fig. 2. mTurquoise was used as a donor and Venus as an acceptor. The N terminal end of synaptosomal-associated protein 25 (SNAP25b) was labelled with either mTurquoise (mtq, a) or in tandem with mtq and Venus (b) to measure the folding fraction of Venus. The binding fractions (or A1 fractions) of syntaxin1A (Syx) with vesicle-associated membrane protein 2 (VAMP2) in the cytosol were detected by mtq－Syx and Venus－VAMP2 (c). The *cis*-complex of Syx with VAMP2 was detected by Syx－mtq and VAMP2－Venus (d), because FRET occurs only when they are present in the same membrane. The assembly of SNAP25 with VAMP2 or Syx was detected by

mtq－SNAP25 and Venus－VAMP2 (e) or Venus－Syx (f). (g) Images of synaptic boutons in rat cortical dissociated culture lipofected with mtq－SNAP25 (scale bar, 5 μm). The left image shows the fluorescence intensity of mtq－SNAP25, while the right image shows the fluorescence decay of the A1 fraction for each pixel in pseudocolour coding shown in j. (h) A lifetime decay curve in a semi-logarithmic plot, which was obtained from eight boutons. The decay fits well with a single exponential function with a time constant of 3.5 ns. (i) The residual data after subtracting the exponential function. (j) Images of synaptic boutons lipofected with the tandem mtq－Venus－SNAP25b probe (scale bar, 5 μm). (k) A lifetime decay curve in a semi-logarithmic plot obtained from 13 boutons, which fits well with a double-exponential function, with time constants of 0.7 ns (τ1) and 3.5 ns (τ2) and weights of 66 % (A1) and 34 % (A2), respectively. (l) The residual data after subtracting the A2 component (red) or both components (black). (m) The A1 fractions of mtq－SNAP25 (0.28 ± 1.9 %; 19 boutons) and mtq－Venus－SNAP25 probes (63.5 ± 1.2 %; 12 boutons). Wilcoxon signed-rank test versus 0 %: $P = 0.71$ and $^{**}P = 0.002$, respectively.

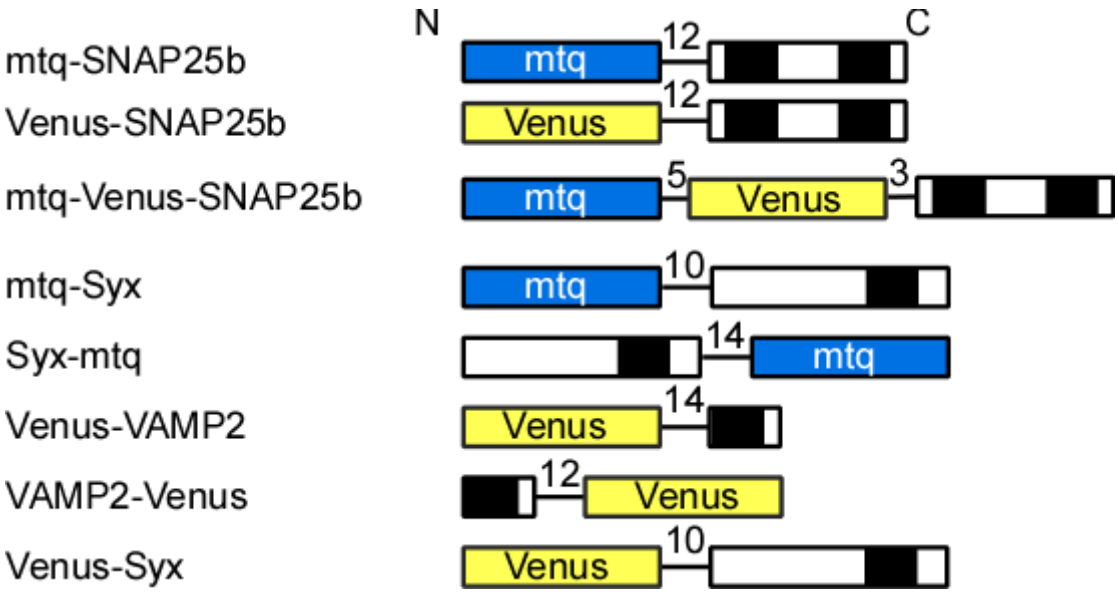

Figure 2 | SNARE Probes for FRET/2pFLIM Analysis Used in the Present Study.
mtq and Venus are in blue and yellow, respectively.
The soluble *N*-ethylmaleimide-sensitive factor attachment protein receptor (SNARE) motifs are in black. The lengths of the linker amino acids between the SNARE motives are indicated.

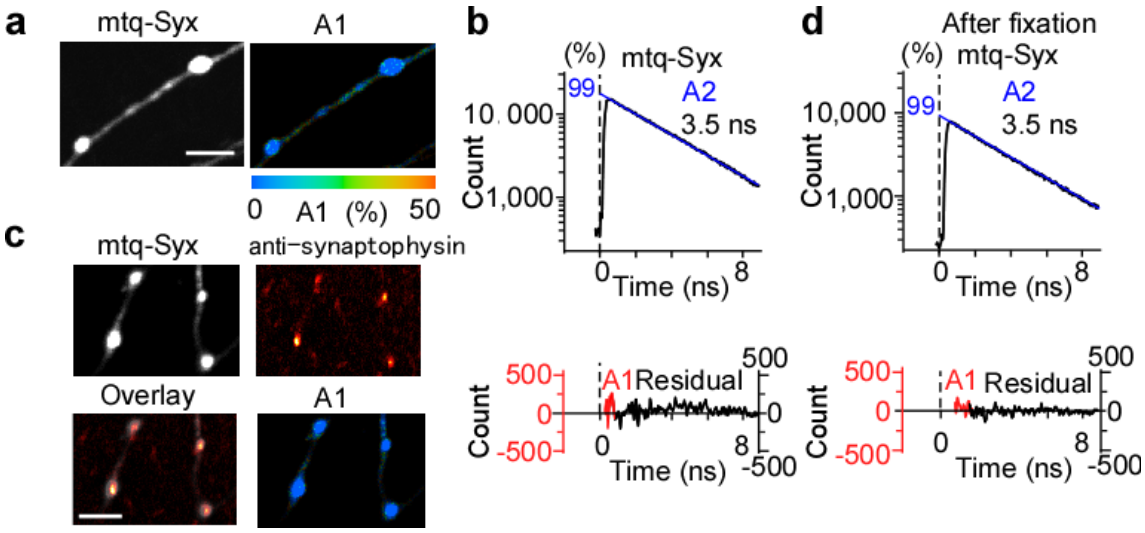

Figure 3 | FRET/2pFLIM of mtq－Syx in live or after fixation.

(a,c) Fluorescence and A1 fraction images of mtq－Syx－expressing boutons (scale bars, 5 μm). Preparations were live-imaged in a and were imaged after chemical fixation and counterstaining with anti-synaptophysin antibody in c. (b,d) Lifetime decay curves of mtq－Syx obtained from 14 boutons.

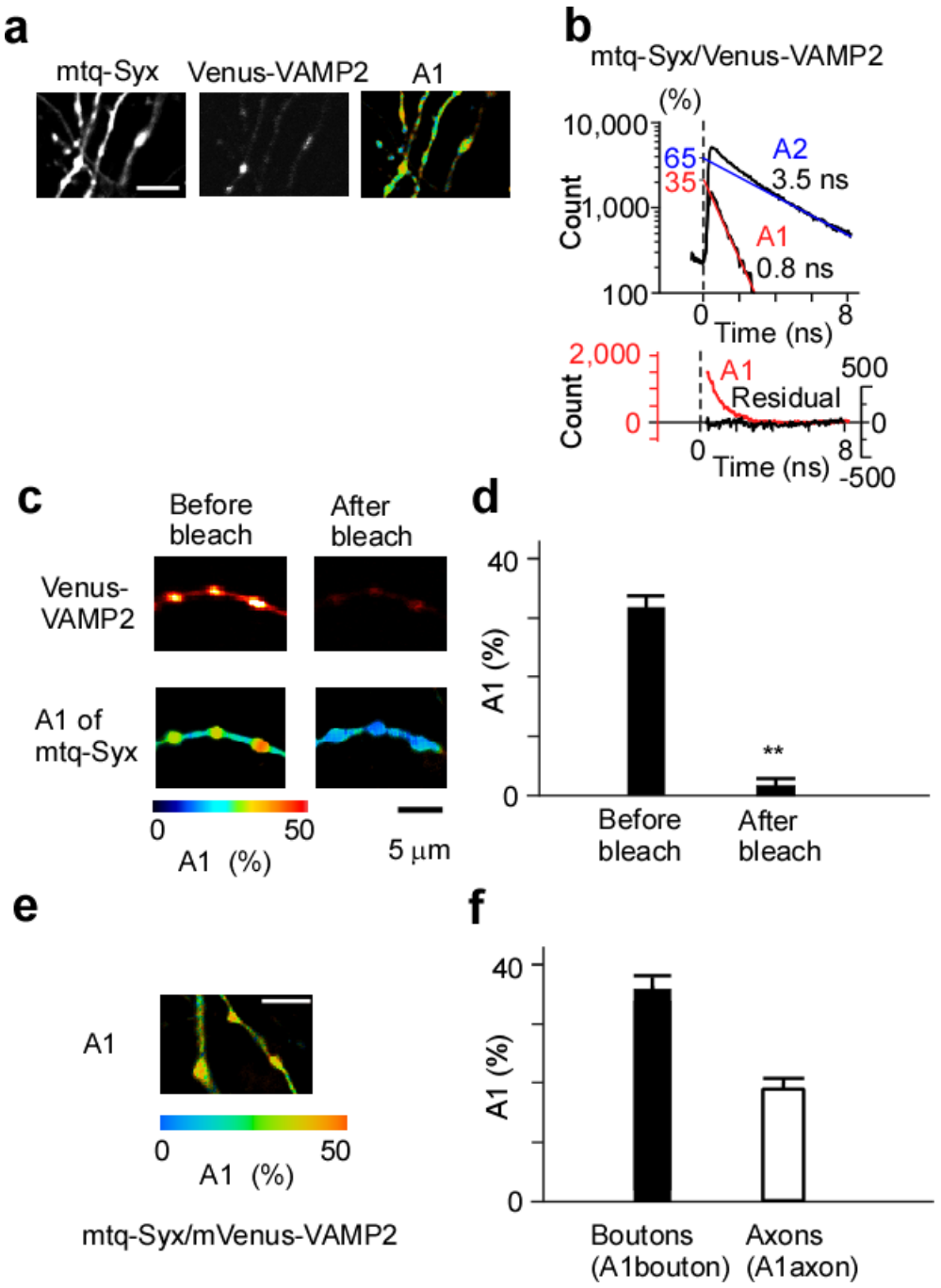

Figure 4 | FRET from mtq－Syx to Venus－VAMP2 detected by 2pFLIM.
(a) Fluorescence and A1 fraction images of mtq－Syx/Venus－VAMP2-stained boutons (scale bars, 5 μm). (b) Lifetime decay curves of mtq－Syx/Venus－VAMP2 obtained from 12 live boutons. (c) Images of Venus fluorescence and the A1 fraction of mtq－Syx before and after photobleaching of Venus in the axonal boutons (scale bar, 5 μm). (d) The A1 fractions of boutons before photobleaching (31.7 ± 1.9 %, 20 boutons) for endogenous expression levels of Venus－VAMP2 expression (mean ± SD = 712 ± 111 A.U.) and after photobleaching (1.8 ± 1.1 %) of Venus－VAMP2 (mean

± SD = 198 ± 22 A.U). **P = 0.0004 with the Mann–Whitney U-test. (e) An image of the A1 values of mtq－Syx for mVenus－VAMP2 (scale bar , 5 μm). (f) The A1 values obtained by mtq－Syx/mVenus－VAMP2 in bouton (36.3 ± 2.2 %, 12 boutons:A1bouton) with the expression level of mVenus of 46-185 % endogenous level (mean ± SD = 587 ± 69 A.U.) and in axon (19.4 ± 1.5 %, 11 axons : A1axon), which are not significantly different from those obtained by mtq－Syx/Venus－VAMP2 (see Fig. 11c; P = 0.56 and 0.25 in boutons and axons, respectively).

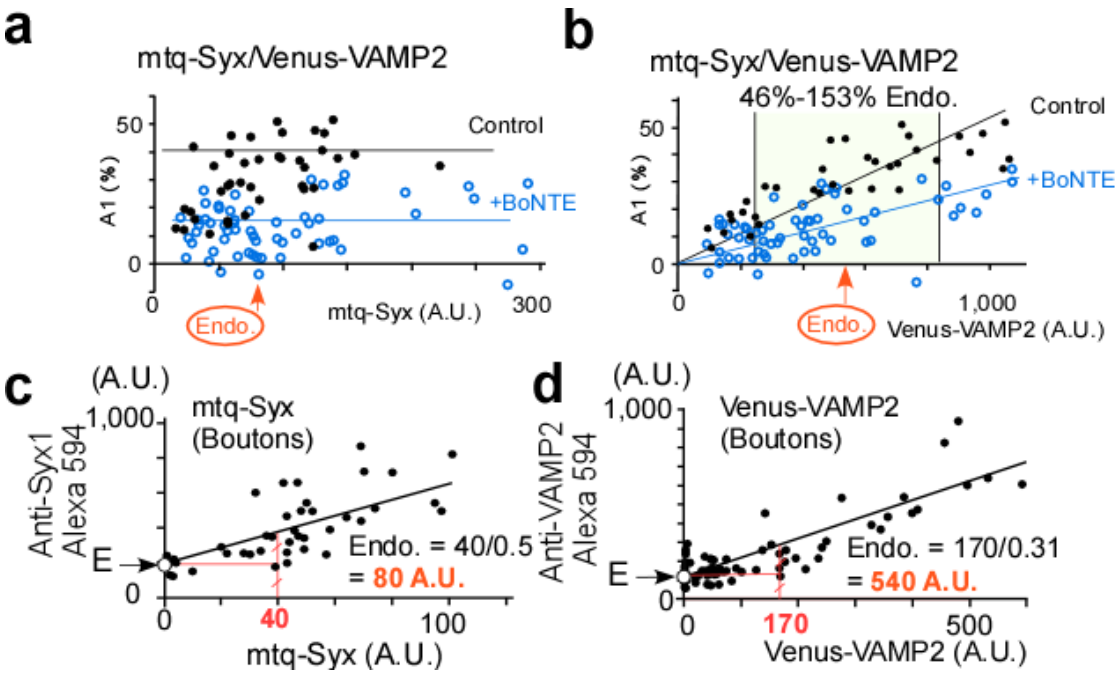

Figure 5 | The Dependence of the A1 Fractions on the Expression Levels of FRET Acceptors in the Neurons.

The A1 values for mtq－Syx/Venus－VAMP2 (a,b) plotted against the expression levels of mtq－Syx (arbitrary unit) of each probe in each bouton in the absence and presence of clostridial toxins. The endogenous expression levels of each SNARE protein, obtained from c, d, are indicated with red ovals denoted as 'Endo.' (c,d) Fluorescence intensities of boutons stained with anti-SNARE antibodies are plotted against the fluorescence intensity of the same proteins labelled either with Venus or mtq for boutons in rat dissociated culture (n = 69, 51).

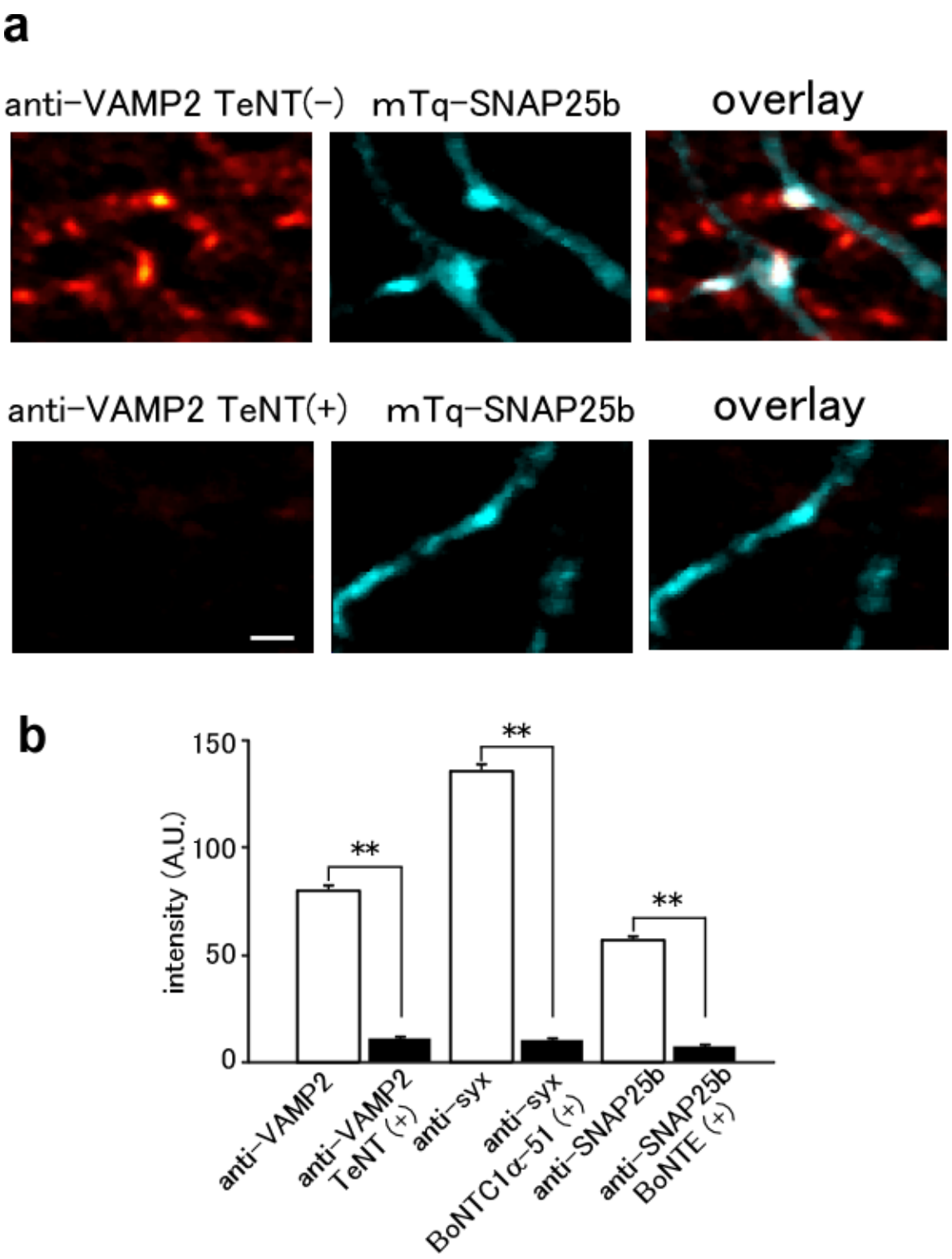

Figure 6 | Specificity of antibodyes against VAMP2, Syx and SNAP25.
(a) Images of anti-VAMP2 conjugated with Alexa594, mtq－SNAP25b and their overlays in dissociated culture preparations without and with expression of the light chain of TeNT (scale bar, 2 μm). (b) Alexa fluorescence intensities conjugated with anti-VAMP2 antibody in control (80.3 ± 2.6 A.U., 20 boutons) and in TeNT (11.1 ±

0.79 A.U., 20 boutons), with anti-Syx antibody (135.7 ± 3.4 A.U., 20 boutons) and in BoNTC1α-51 (10.6 ± 1.1 A.U., 20 boutons), and with anti-SNAP25b (57.0 ± 2.1 A.U., 20 boutons) and in BoNTE (7.4 ± 1.1 A.U., 20 boutons). $^{**}P < 0.001$ with the Mann–Whitney *U*-test.

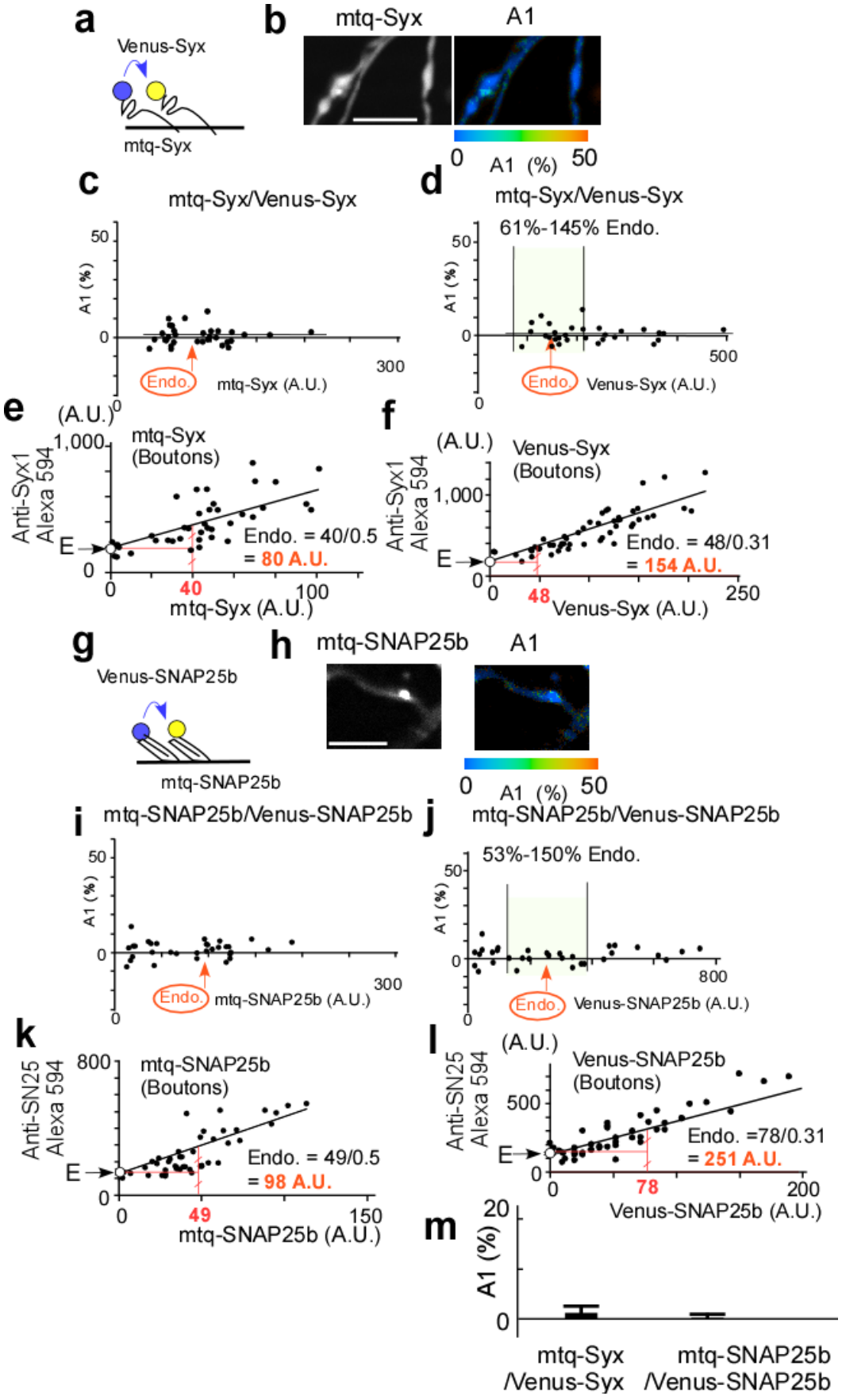
a
Venus-Syx
mtq-Syx
b
mtq-Syx
A1
0
A1 (%)
50
c
mtq-Syx/Venus-Syx
A1 (%)
50
0
300
Endo.
mtq-Syx (A.U.)
d
mtq-Syx/Venus-Syx
61%-145% Endo.
A1 (%)
50
0
500
Endo.
Venus-Syx (A.U.)
e
(A.U.)
mtq-Syx
(Boutons)
Anti-Syx1
Alexa 594
1,000
E
0
Endo. = 40/0.5
= 80 A.U.
0
40
100
mtq-Syx (A.U.)
f
(A.U.)
Venus-Syx
(Boutons)
Anti-Syx1
Alexa 594
1,000
E
0
Endo. = 48/0.31
= 154 A.U.
0
48
250
Venus-Syx (A.U.)
g
Venus-SNAP25b
mtq-SNAP25b
h
mtq-SNAP25b
A1
0
A1 (%)
50
i
mtq-SNAP25b/Venus-SNAP25b
A1 (%)
50
0
300
Endo.
mtq-SNAP25b (A.U.)
j
mtq-SNAP25b/Venus-SNAP25b
53%-150% Endo.
A1 (%)
50
0
800
Endo.
Venus-SNAP25b (A.U.)
k
800
mtq-SNAP25b
(Boutons)
Anti-SN25
Alexa 594
E
0
Endo. = 49/0.5
= 98 A.U.
0
49
150
mtq-SNAP25b (A.U.)
l
(A.U.)
Venus-SNAP25b
(Boutons)
Anti-SN25
Alexa 594
500
E
0
Endo. =78/0.31
= 251 A.U.
0
78
200
Venus-SNAP25b (A.U.)
m
20
A1 (%)
0
mtq-Syx
/Venus-Syx
mtq-SNAP25b
/Venus-SNAP25b

Figure 7｜FRET/2pFLIM analysis of homotypic Syx or SNAP25 binding.
(a) Schematic drawing of mtq－Syx/Venus－Syx. (b) Fluorescence and A1 images of mtq－Syx/Venus－Syx-expressing boutons (scale bar, 5 μm). (c,d) The A1 values among boutons with various expression levels of Syx and SNAP25. The green shaded area was used to obtain the A1 value for the endogenous expression level of the acceptor Syx of 154 A.U.: 61 %–145 % (d, mean ± SEM = 148 ± 8 A.U., n = 16). (e,f) Fluorescence intensities of boutons stained with anti-SNARE antibodies are plotted against the fluorescence intensity of the same proteins labelled either with Venus for boutons in rat dissociated culture (e,f; n = 51, 51). (g) Schematic drawing of mtq－SNAP25/Venus－SNAP25. (h) Fluorescence and A1 images of mtq－SNAP25/Venus－SNAP25-expressing boutons (scale bar, 5 μm). (i,j) The A1 values among boutons with different expression levels of mtq－SNAP25b (i) or Venus－SNAP25b (j). The green shaded area was used to obtain the A1 value for the endogenous expression level of the acceptor SNAP25 of 262 A.U.: 53 %–150 % (i, mean ± SD = 251 ± 23 A.U., n = 13). (k,l) Fluorescence intensities of boutons stained with anti-SNARE antibodies are plotted against the fluorescence intensity of the same proteins labelled either with Venus for boutons in rat dissociated culture (e,f; n = 46, 43). (m) The A1 values of mtq－Syx/Venus－Syx (1.2 ± 1.4 %, n = 16) and mtq－SNAP25b/Venus－SNAP25b (1.4 ± 1.1 %, n = 13) with the endogenous expression levels of Syx and SNAP25, respectively (e,f). Wilcoxon signed-rank test versus 0 %: $P = 0.63$ and $P = 0.17$, respectively.

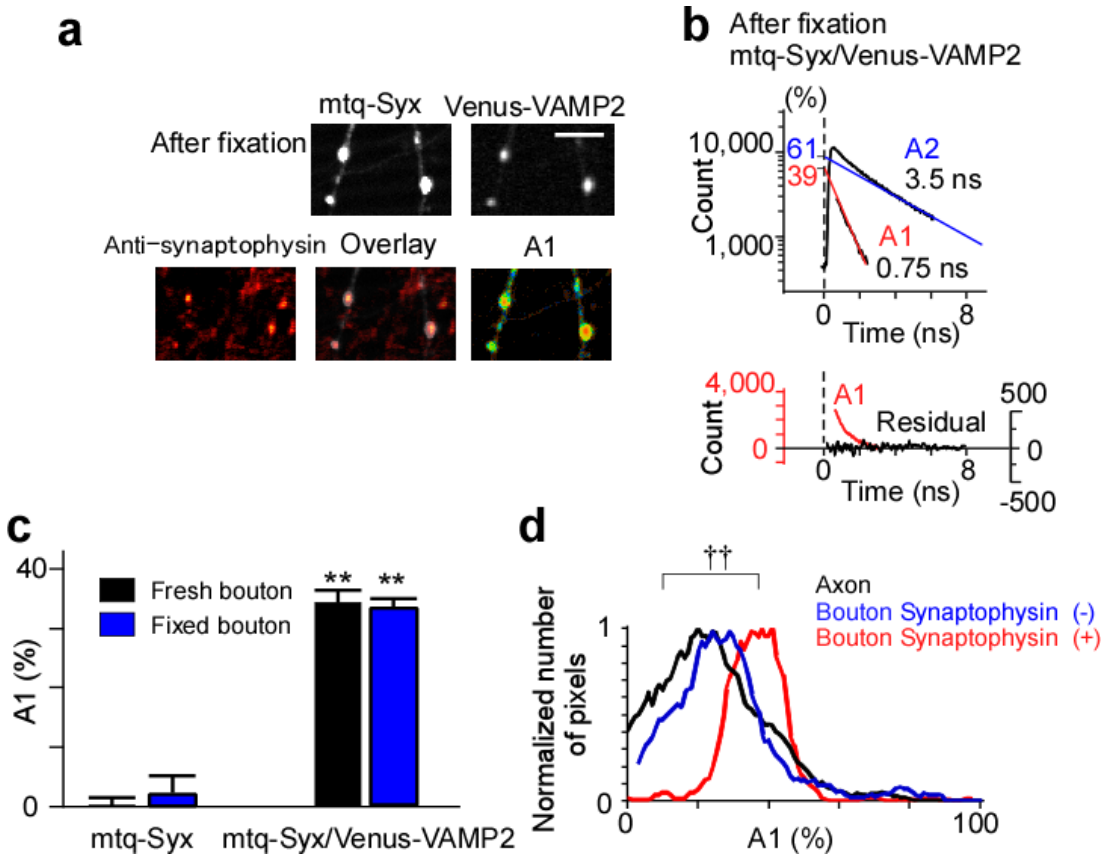

Figure 8 | FRET/2pFLIM of the SNARE complexes between mtq−Syx and Venus −VAMP2 in neurons.

(a) Fluorescence and A1 fraction images of mtq−Syx/Venus−VAMP2-expressing boutons (scale bars, 5 μm). Preparations were after chemical fixation and counterstaining with anti-synaptophysin antibody. (b) Lifetime decay curves of mtq−Syx/Venus−VAMP2 obtained from 12 live boutons and 8 fixed boutons. (c) The A1 fractions of mtq−Syx (black bar; 0.18 ± 1.4 %; 14 boutons) or after fixation (blue bar; 2.4 ± 2.9 %; 14 boutons) and mtq−Syx/Venus−VAMP2 stained boutons in live images (black bar; 34.1 ± 2.0 %; 21 boutons) and after fixation (blue bar; 33.2 ± 1.3 %; 19 boutons) at the endogenous expression level of VAMP2 (Fig. 5d). The A1 fractions for mtq−Syx/Venus−VAMP2 were signi ficantly different from 0 % (***P* = 0.0004 and ***P* = 0.0001 using the Wilcoxon signed-rank test). The A1 fraction was not affected by fixation (*P* = 0.74 using the Mann–Whitney *U*-test). (d) Distributions of the A1 fractions in the boutons among the pixels positive (red; 38.8 ± 1.8 %; 519 pixels) or negative (blue; 17.4 ± 2.2 %; 323 pixels) for anti-synaptophysin staining or in axons (black; 15.6 ± 2 %; 183 pixels; *P*=0.0002 using the Kruskal–Wallis test; *P* = 0.75 and $^{\dagger\dagger}P$ = 0.0039 for boutons negative and positive for synaptophysin versus axons using Steel's test).

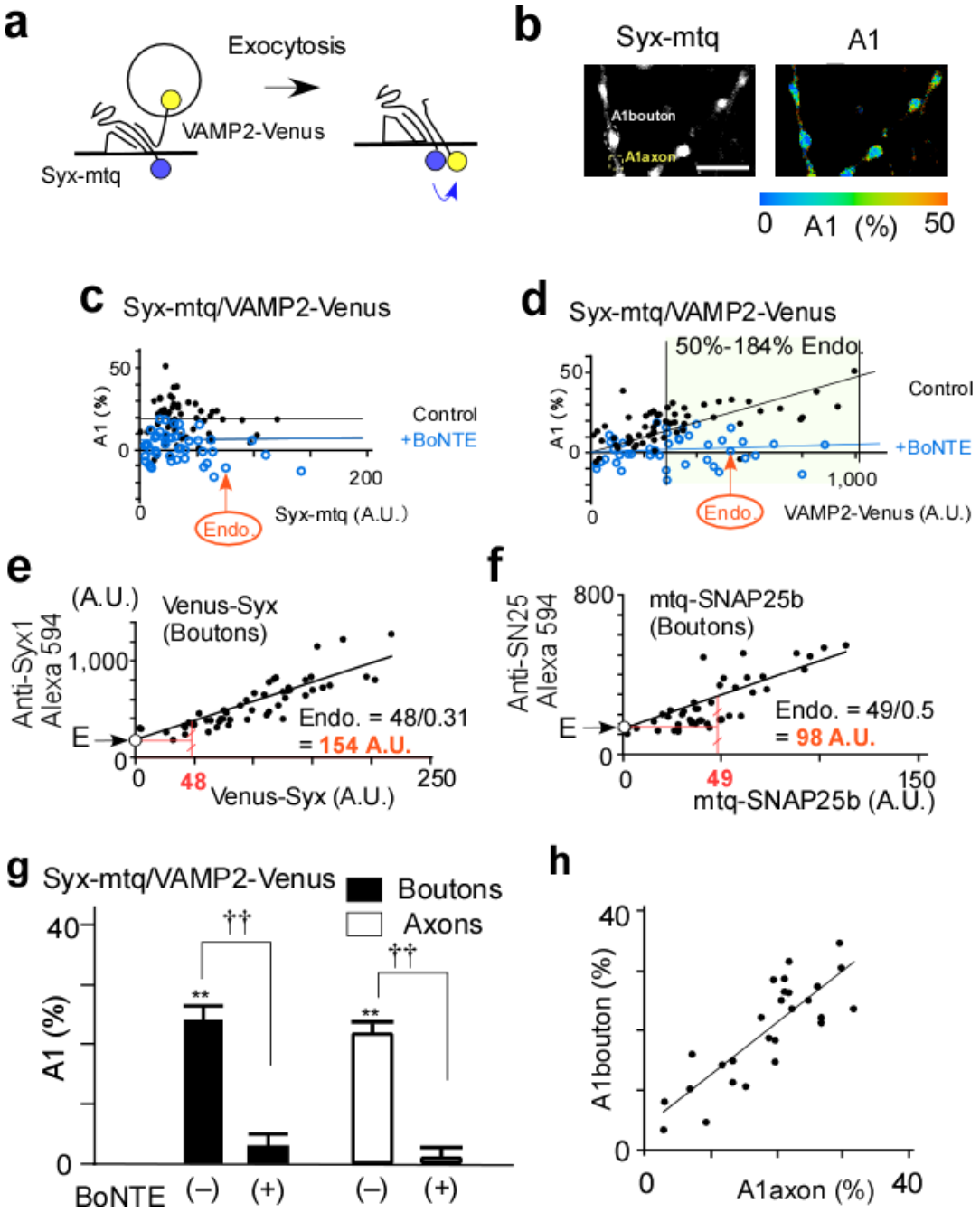

Figure 9 FRET/2pFLIM of *cis*-SNARE complexes between Syx－mtq and VAMP2－Ven in neurons.

(a) Schematic drawing of the conformation change of the *cis*-probes via exocytosis. (b) Fluorescence and A1 fraction images of Syx－mtq/VAMP2－Venus-expressing boutons (scale bar, 5 μm). (c,d) The A1 values for Syx－mtq/VAMP2－Venus plotted against the expression levels of Syx－mtq and VAMP2－Venus (arbitrary unit) of each probe in each bouton in the absence and presence of BoNTE. The endogenous expression levels of each SNARE protein, obtained from (e,f) are indicated with red ovals denoted as 'Endo.'. (e,f) Fluorescence intensities of boutons stained with

anti-SNARE antibodies are plotted against the fluorescence intensity of the same proteins labelled either with Venus or mtq for boutons in rat dissociated culture. (g) The average A1 fractions of Syx－mtq/VAMP2－Venus-stained boutons (black) and axons (open) in the absence and presence of the light chain of botulinum toxin (BoNTE). The A1 fractions in boutons (24.7 ± 2.1 %; 24 boutons) and axons (21.5 ± 2.0 %; 19 axons) were significantly different from 0 % (**P = 0.0001 and 0.00001 using the Wilcoxon signed-rank test) in the absence of BoNTE at the mean expression levels of VAMP2—Ven of 524 ± 45 A.U. and 508 ± 26 A.U., respectively (Fig. 9d). They were not significantly different from 0 % in the boutons (3.5 ± 2.1 %; 22 boutons) and axons (0.9 ± 2 %; 12 axons) in the presence of BoNTE using the Wilcoxon signed-rank test (P = 0.12 and 0.53). The Mann–Whitney U-test yielded $^{\dagger\dagger}P$ = 0.00001 for boutons without and with toxin, and $^{\dagger\dagger}P$ = 0.00001 for axons. (h) The correlation between the A1 fractions in the boutons (A1bouton) and those of axons surrounding the boutons (A1axon; P = 0.0001 using Spearman's rank correlation coefficient; r = 0.80; n = 27).

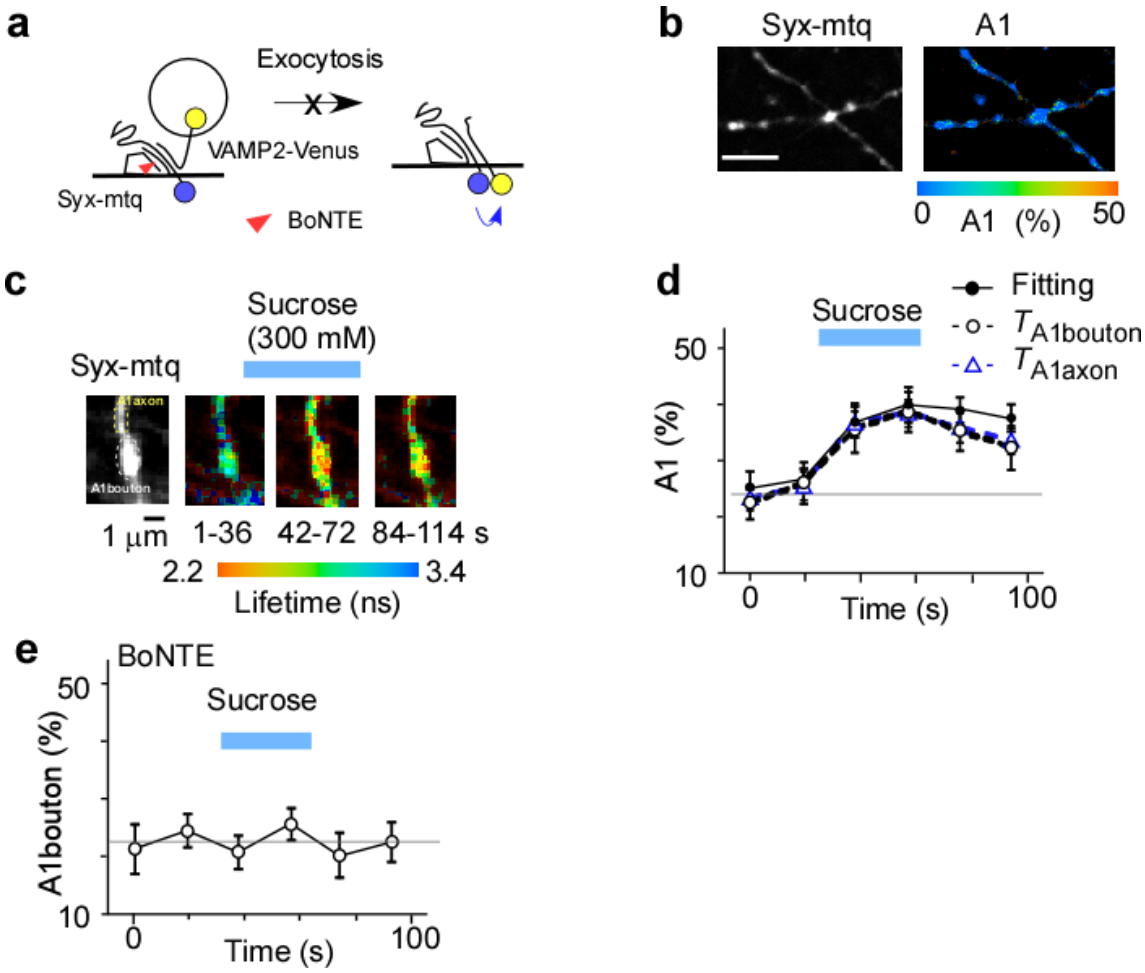

Figure 10. Sucrose stimulation of preparations staning with the *cis*-probe in the absence and presence of BoNTE.

(a) Schematic illustaration of the action of BoNTE on exocytosis.

(b) Fluorescence and A1 fraction images of boutons expressing Syx－mtq, VAMP2－Venus and BoNTE (scale bar, 5 μm). (c) Fluorescence lifetime images of Syx－mtq/VAMP2－Venus-stained boutons during 300 mM sucrose stimulation (scale bar, 1 μm). (d) The time courses of the A1 fractions estimated either by decay curve fitting (filled circles, 21 boutons) or average lifetimes (open symbols, 21 boutons) in the boutons ($T_{A1bouton}$, open circles, n = 19) and axons surrounding the boutons (T_{A1axon}, open triangles). All values after sucrose stimulation were significantly ($P < 0.01$) different from those before stimulation. (e) The time courses of A1bouton estimated by average lifetimes during 300 mM sucrose stimulation in the preparation treated with BoNTE (n = 19).

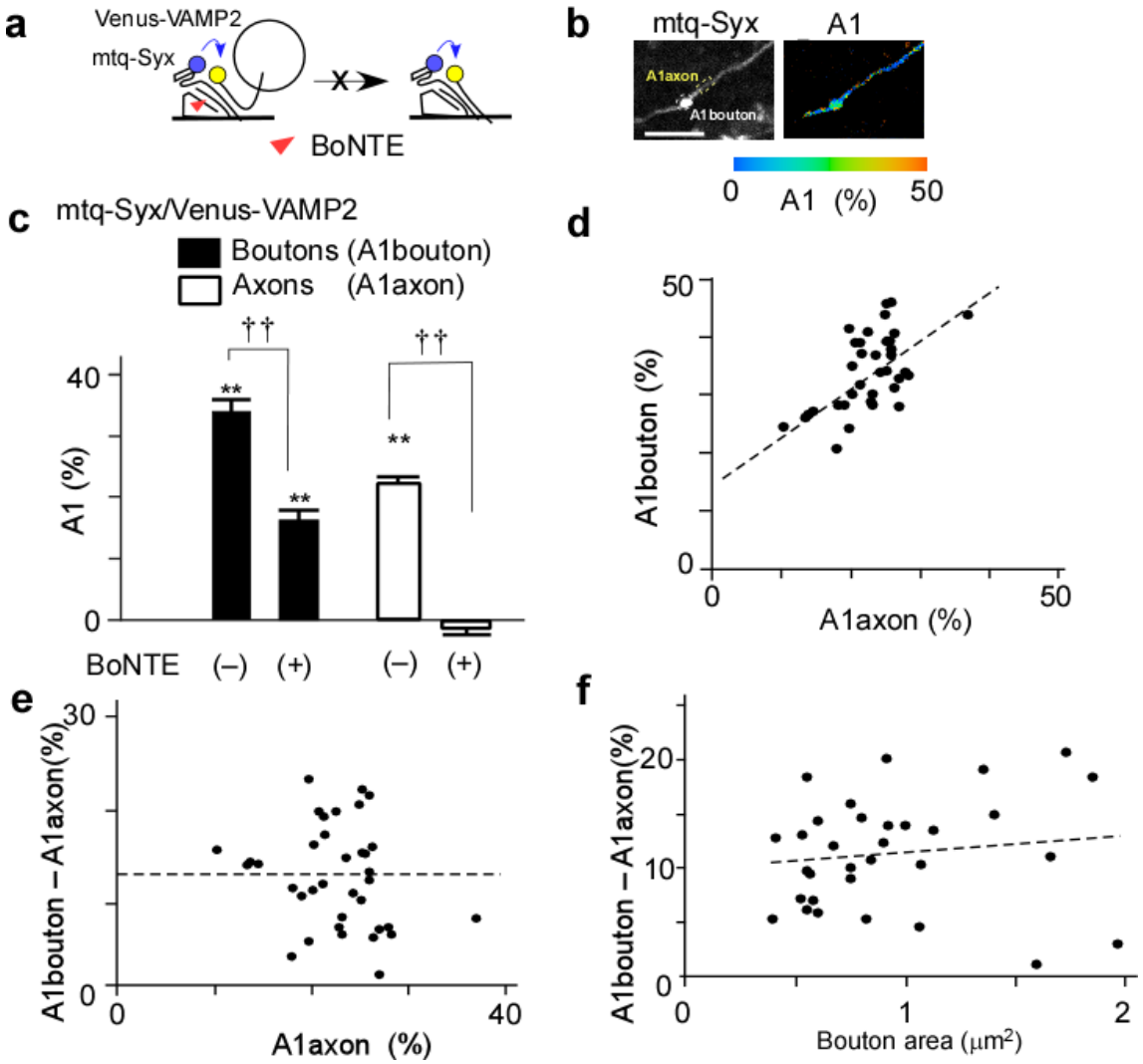

Figure 11 | Action of the light chain of botulinum toxin E (BoNTE) on the SNARE complexes.

(a) Schematic drawing of the *trans*-complex with mtq－Syx/Venus－VAMP2 and the site of action of the light chain of BoNTE, which blocks exocytosis and the formation of the *cis*-complex. (b) Fluorescence and A1 fraction images of boutons simultaneously lipofected with mtq－Syx, Venus－VAMP2 and BoNTE (scale bar, 5 μm). (c) The A1 fractions of boutons in the absence and presence of BoNTE (16.3 ± 1.6 %, 39 boutons) at the endogenous expression level of VAMP2 (Fig. 5b) and of axons in the absence (open bars, 22.4 ± 0.9 %; 33 axons) and in the presence of BoNTE (-1.9 ± 1.8 %; 17 axons). Wilcoxon signed-rank test versus 0 %: $^{**}P = 0.0001$ in BoNTE-treated boutons, whereas $^{**}P = 0.0003$ and $P = 0.42$ in axons untreated or treated with BoNTE. The A1 fraction values of BoNTE versus control in boutons and axons differed with

$^{\dagger\dagger}P = 0.0006$ and $^{\dagger\dagger}P = 0.004$ using the Mann–Whitney *U*-test, respectively.
(d) The correlation between the A1 fractions of individual boutons (A1bouton) and those in the surrounding axons (A1axon; $P = 0.0012$ using Spearman's rank correlation coefficient; r = 0.59; n = 36). (e) The correlation between (A1bouton–A1axon) and A1axon ($P = 0.21$ using Spearman's rank correlation coefficient; r = -0.23, n = 36). (f) The correlation between (A1bouton–A1axon) and the bouton area in its central Z-section ($P = 0.20$ using Spearman's rank correlation coefficient; r = 0.13, n = 32).

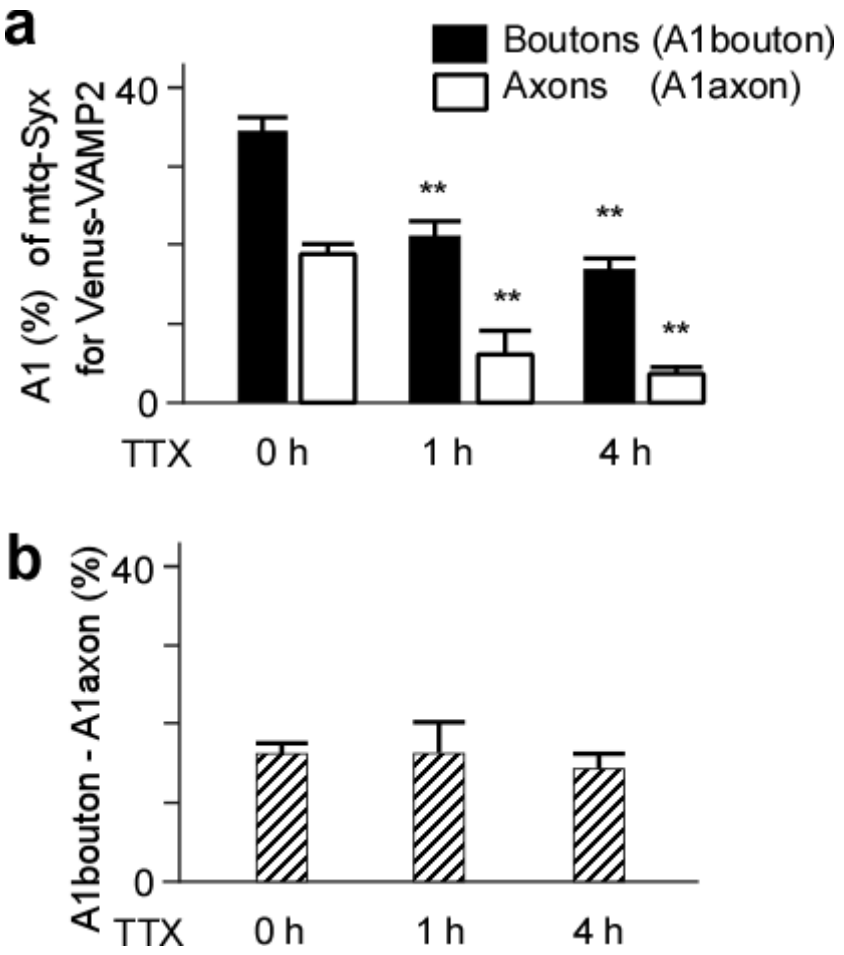

Figure 12｜TTX effects on the A1 fractions for mtq－Syx/Venus－VAMP2.
(a) The A1 fractions (34.5 ± 1.8 %, 16 boutons; 18.9 ± 1.8 %, 21 axons) in control, and those (20.9 effici %, 21 boutons; 6.1 ± 3.0 %, 12 axons) 1 h after treatment of TTX, and those (16.9 ± 1.4 %, 23 boutons; 3.6 ± 0.9 %, 10 axons) 4 h after treatment of TTX. ** $P < 0.001$ with the Mann–Whitney *U*-test vs. 0 h. (b) The *trans*-SNARE fractions obtained by the gradient method in control (16.0 ± 1.2 %, 15 boutons), 1 h after TTX treatment (16.0 ± 4.2 %, 11 boutons) and 4 h after (14.1 ± 1.9 %, 10 boutons).

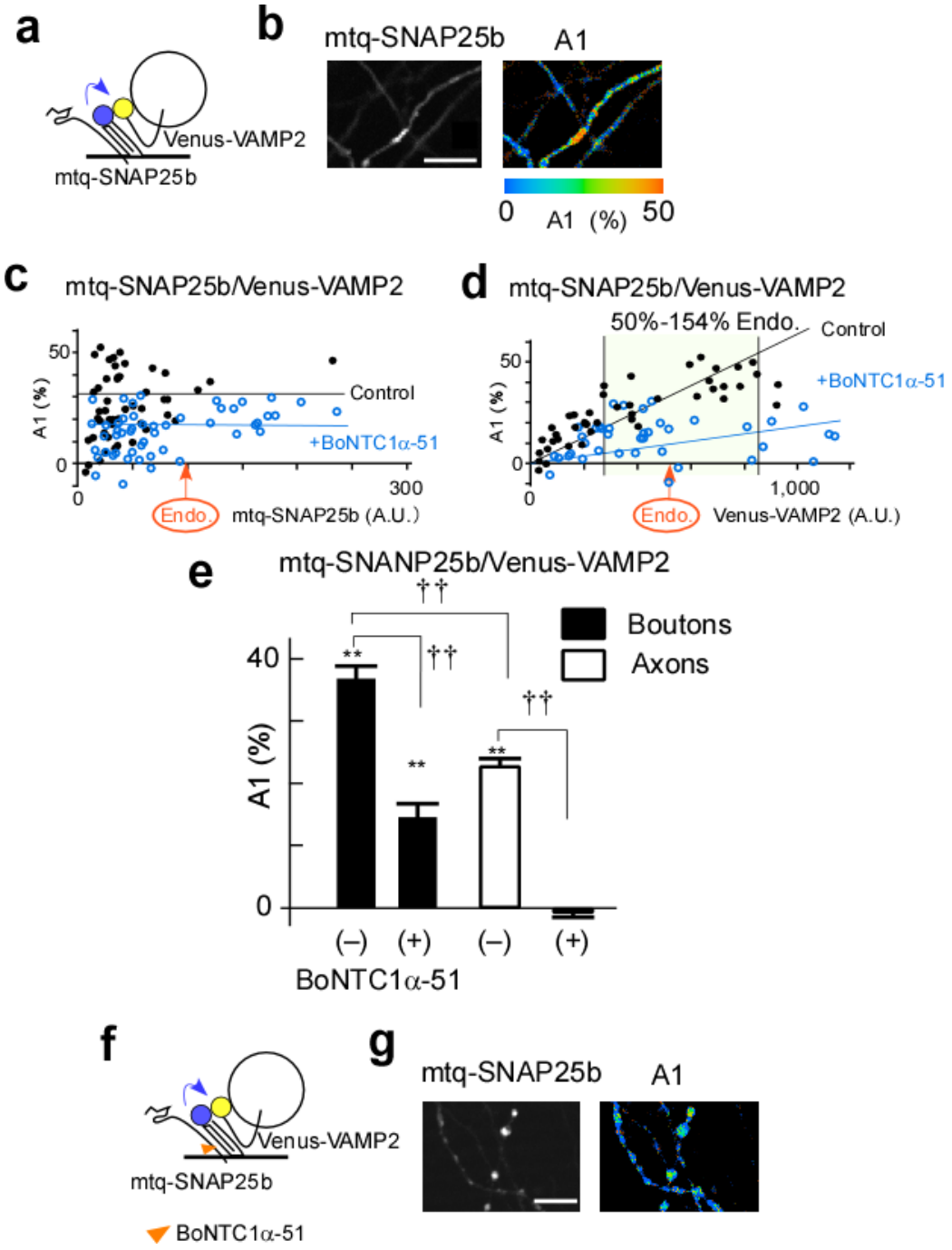

Figure 13 | FRET/2pFLIM of mtq－SNAP25-based probes for SNARE complexes. (a) Schematic drawing of mtq－SNAP25/Venus－VAMP2 probes. (b) Fluorescence and A1 fraction images of mtq－SNAP25/Venus－VAMP2 expressing boutons (scale bars, 5 μm). (c,d) The A1 values for mtq－SNAP25/Venus－VAMP2 plotted against the expression levels of mtq－SNAP25 (c) and Venus－VAMP2 (d) (arbitrary unit) in the absence and presence of BoNTC1α-51. (e) The A1 fractions of mtq－SNAP25/Venus－VAMP2-expressing boutons (filled; 36.7 ± 2.2 %; 20 boutons at the endogenous expression level of VAMP2; Fig. 5d) and axons (open; 22.7 ± 1.3 %;

22 axons) and those in the presence of BoNTC1α-51 in boutons (14.5 ± 2.2 %; 24 boutons) and in axons (-0.4 ± 1.1 %; 17 axons). $^{**}P < 0.001$ for control boutons and axons and $^{**}P = 0.0001$ for BoNTC1α-51-treated boutons using the Wilcoxon signed-rank test versus 0 %. Using the Kruskal–Wallis test on the four groups, I obtained a P value of < 0.00001, and the effects of BoNTC1α-51 on boutons and axons were $^{\dagger}P = 0.03$ and $^{\dagger}P = 0.04$, respectively, using Scheffé's test. $^{\dagger\dagger}P = 0.004$ between control boutons and axons and $^{\dagger\dagger}P = 0.002$ between BoNTC1α-51-treated boutons and axons. (f) Schematic drawing of mtq－SNAP25/Venus－VAMP2 probes and the action of BoNTC1α-51.
(g) Fluorescence and A1 fraction images of mtq－SNAP25/Venus－VAMP2-expressing boutons in the absence (g) and presence of tetanus toxin (BoNTC1α-51) (scale bars, 5 μm).

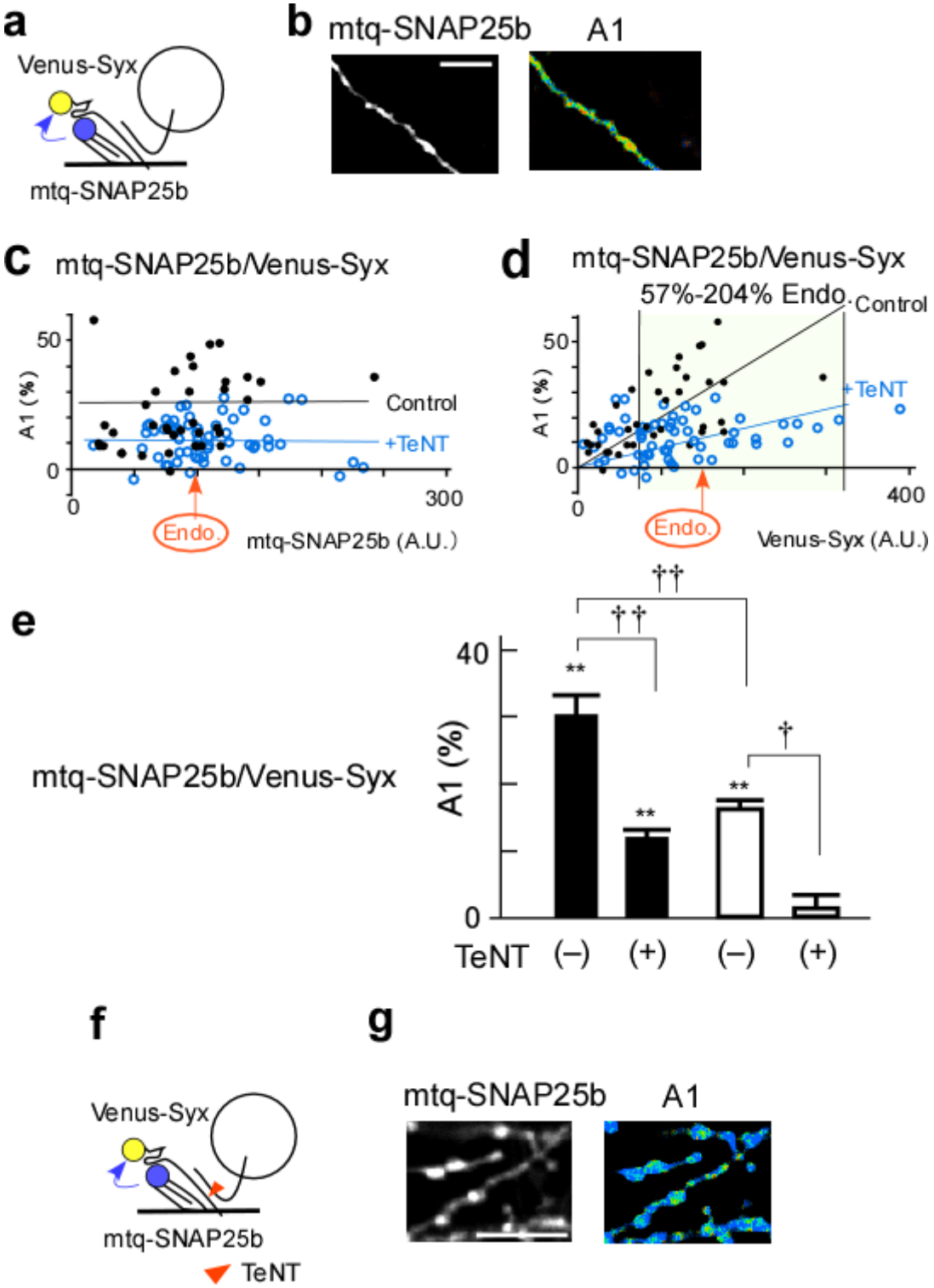

Figure 14 | FRET/2pFLIM of mtq－SNAP25-based probes for SNARE complexes. (a) Schematic drawing of mtq－SNAP25/Venus－Syx probe. (b) Fluorescence and A1 fraction images of mtq－SNAP25/Venus－Syx expressing boutons (scale bars, 5 μm). (c,d) The A1 values for mtq－SNAP25/Venus－Syx plotted against the expression levels of mtq－SNAP25 (c) and Venus－Syx (d) (arbitrary unit) in the absence and

presence of TeNT. (e) The average A1 fractions of mtq－SNAP25/Venus－Syx-stained boutons (filled; 29.5 ± 3.1 %; 21 boutons with the mean expression of Venus－Syx of 139 A.U.; Fig. 7f) and axons (open; 16.2 ± 1.3 %; 28 axons), those of boutons in the presence of TeNT (12.0 ± 1.1 %; 45 boutons with the mean expression level Venus－Syx of 138 A.U.) and of axons (2.4 ± 1.7 %; 15 axons). $^{**}P < 0.01$ for control boutons, axons and TeNT-treated boutons using the Wilcoxon signed-rank test versus 0 %. Using the Kruskal–Wallis test on the four groups, I obtained a P value of < 0.00001. The A1 values of boutons and axons were different ($^{\dagger\dagger}P = 0.004$) in the absence of the toxin, and the toxin's effects were significant: $^{\dagger\dagger}P = 0.0007$ and $^{\dagger}P = 0.04$ for boutons and axons using Scheffé's test. (f) Schematic drawing of the action of TeNT on mtq－SNAP25/Venus－Syx probe. (g) Fluorescence and A1 fraction images of mtq－SNAP25/Venus－Syx expressing boutons (scale bars, 5 μm).

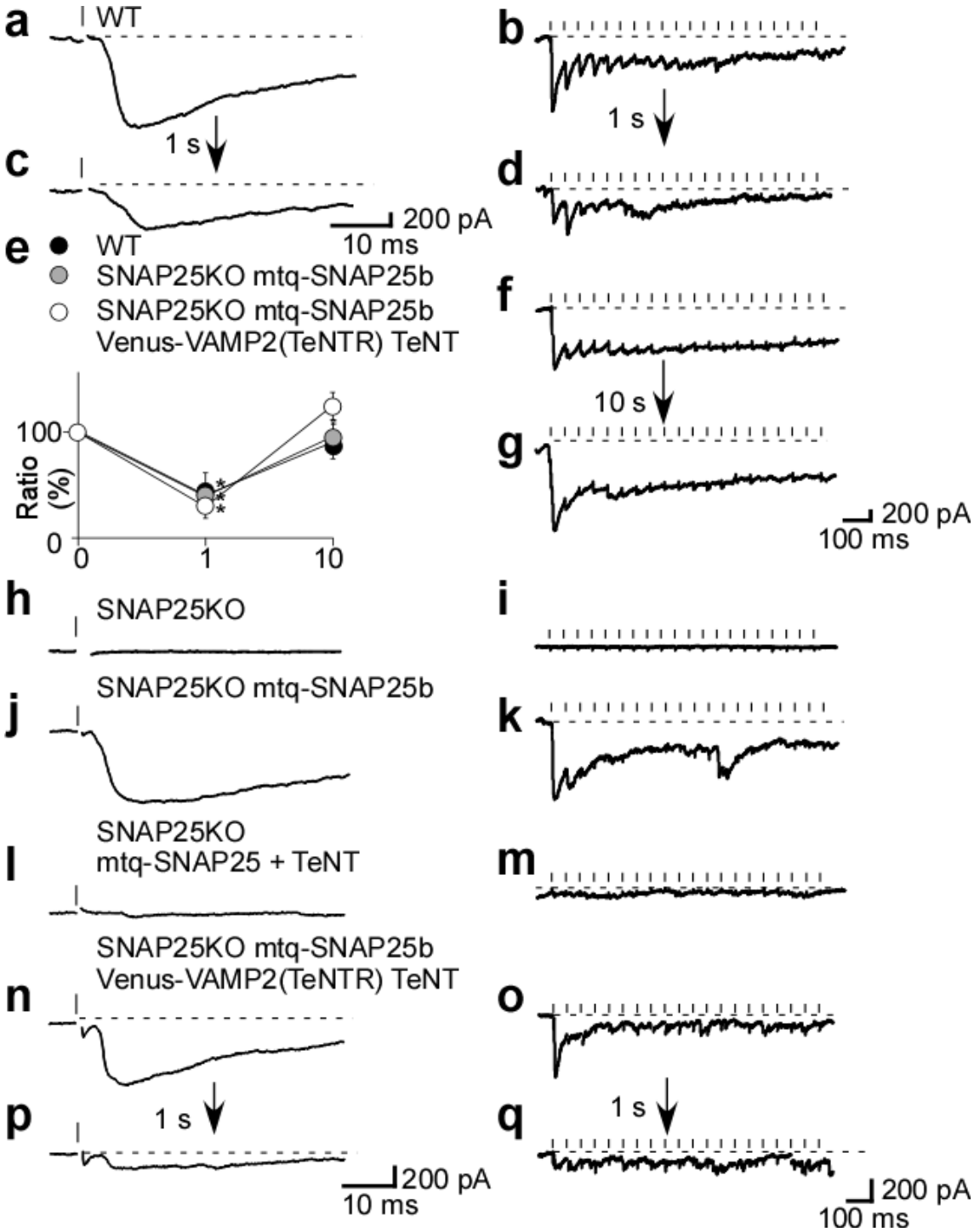

Figure 15 | Kinetics of EPSCs, depletion and refilling of vesicles mediated by mtq－SNAP25b/Venus－VAMP2 in SNAP25 KO mice treated with TeNT.

(a,b) EPSCs recorded from dissociated cultures from wild-type (WT) mice after the first stimulation (a) and during 20 repetitive stimuli at 20 Hz in the presence of picrotoxin (50 μM) and cyclothiazide (100 μM). The current traces were recorded with whole-cell patch clamp, and presynaptic fibres were stimulated with a glass electrode. (c,d) EPSCs evoked from the same cell by the second repetitive stimulation 1 s after the first train of

stimuli. (e) Amplitudes of the first EPSCs in the repetitive stimulation relative to that of the first train of stimulation. Two trains were separated by 1s in the preparations from WT mice (filled circles, 40 ± 21 %, n = 6, $P = 0.04$), those from the KO mice rescued with mtq－SNAP25b (grey circles, 29 ± 8.5 %, n = 5, $P = 0.043$), and those from the KO mice expressing mtq－SNAP25b and Venus－VAMP2 (TeNT resistant) after treatment with TeNT (open circles, 39 ± 12 %, n = 8, $P = 0.01$). The P values were obtained with the Wilcoxon signed-rank test. The amplitudes recovered to 91 ± 16 % (n = 6, $P = 0.6$), 96 ± 13 % (n = 4, $P = 0.1$), and 125 ± 13 % (n = 4, $P = 0.9$) when the interval was set to 10 s. (f,g) EPSCs evoked by the first (f) and second (g) repetitive stimulation separated by 10 s. (h—m) EPSCs recorded from dissociated cultures obtained from SNAP25 KO mice (h,i), those rescued by mtq－SNAP25b (n = 8) (j,k) and those with exocytosis blocked by TeNT treatment (n = 8) (l,m). (n—q) Current traces recorded from dissociated culture preparations from SNAP25 KO mice expressing mtq－SNAP25 and Venus－VAMP2(TeNTR), and treated with TeNT for 1 day. The first and second repetitive stimuli were separated by 1 s.

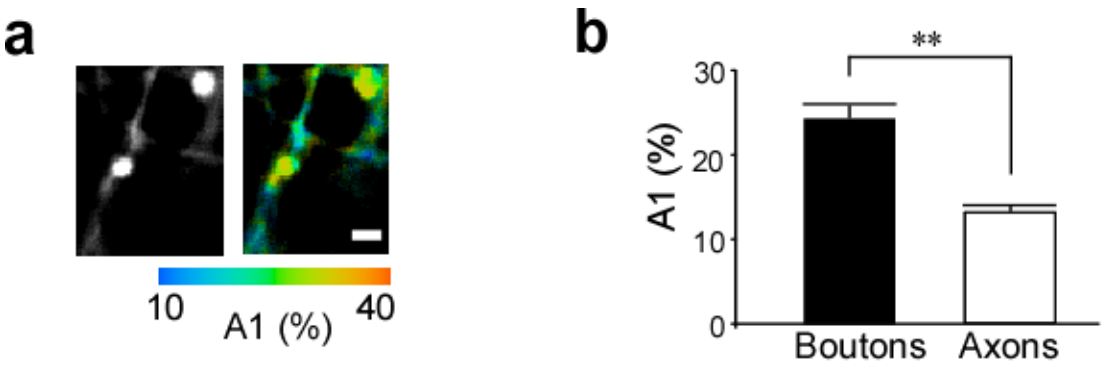

Figure 16 | FRET/FLIM images of mtq－SNAP25b/Venus－VAMP2 in SNAP25 KO mice treated with TeNT.

(a) Fluorescence and A1 images of mtq－Syx/Venus－VAMP2(TeNTR)-expressing boutons (scale bar, 1 μm). (b) The mean A1 values in boutons (24.4 ± 1.6 %, n = 23) and axons (13.1 ± 0.7 %, n = 35). A Mann–Whitney *U*-test yielded a ***P* value of 0.0000. The average expression levels of mtq－SNAP25 and Venus－VAMP2(TeNTR) were 79 ± 6.7 A.U. and 541 ± 39 A.U., respectively.

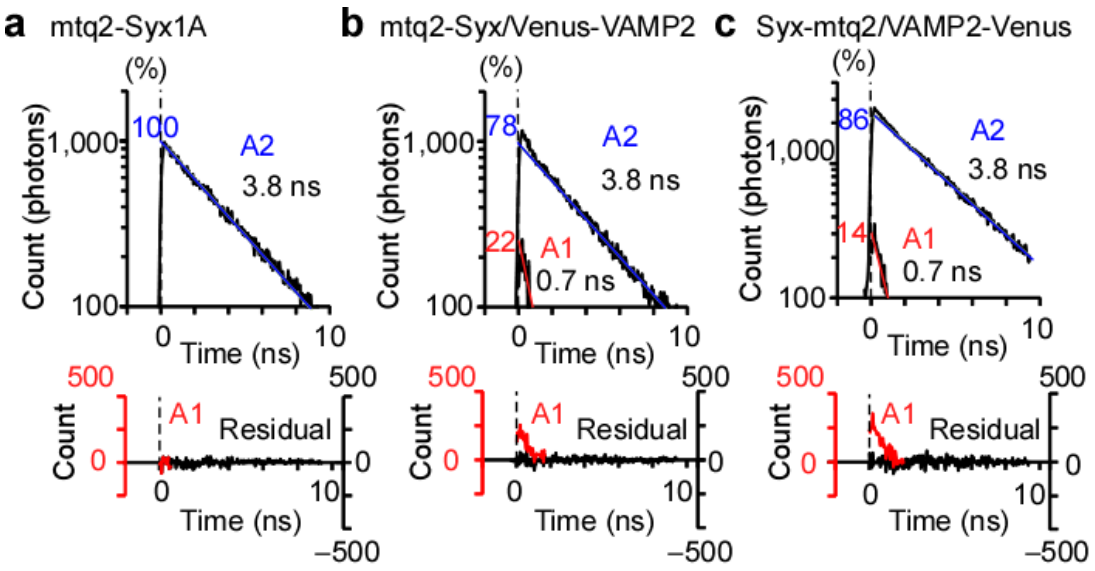

Figure 17 | Lifetime decay curves in boutons of CA1 pyramidal neurons in hippocampal slice cultures.

Slice preparations were transfected with mtq2－Syx (a); mtq2－Syx/Venus－VAMP2 (b); Syx－mtq2/VAMP2－Venus (c) expressed using AAV1/2 virus-mediated gene transfer into the CA3 region, and lifetime decay were analyzed as in Fig. 3b and Fig. 4b. The fluorescence data were accumulated from 8, 38, and 24 boutons. τ_2 was set as 3.8 ns in (a), (b), and (c).

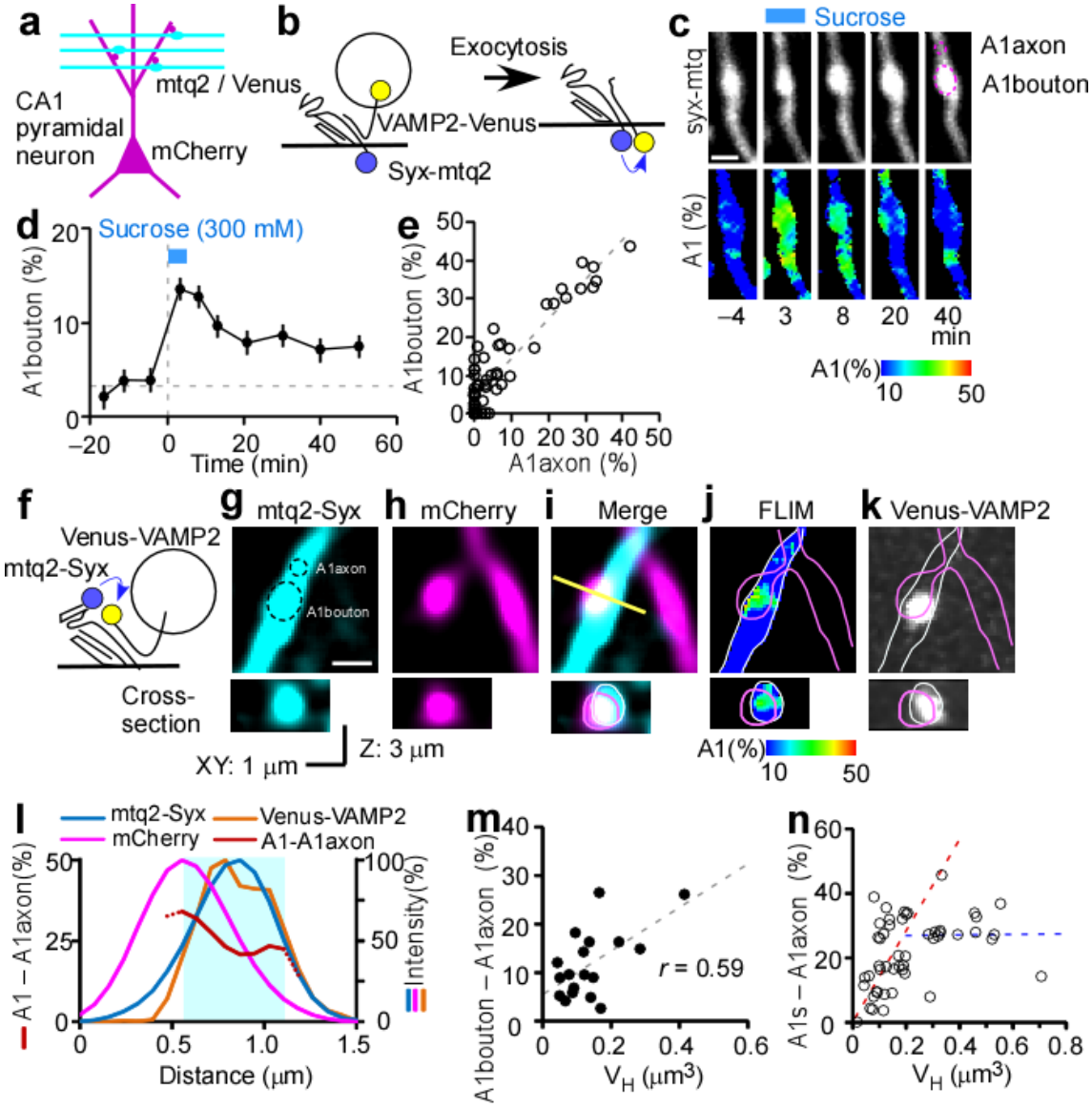

Figure 18 | FRET/2pFLIM of presynaptic boutons on the dendritic spines of CA1 pyramidal neurons in slice culture preparations.

(a) Schematic drawing of Schaffer collateral fibres on CA1 pyramidal neurons in the stratum radiatum. (b) Schematic drawing of *cis*-SNARE probes, Syx－mtq2 and VAMP2－Venus, which induce FRET after exocytosis. (c) Fluorescence lifetime images of Syx－mtq2/VAMP2－Venus-stained boutons during 300 mM sucrose stimulation (scale bar, 1 μm). (d) Average time courses of the A1 fraction in boutons during sucrose application (24 boutons, 8 axons). (e) The correlation between the A1 fractions in the boutons (A1bouton) and those of axons surrounding the boutons (A1axon; $P < 0.0001$ in Spearman's rank correlation coefficient; r = 0.74; n = 59). (f) Schematic drawing of the SNARE probes mtq2－Syx and Venus－VAMP2 in the *trans*-complex. (g,h) Fluorescence images (Z-stacks of three sections) of a Schaffer collateral axon expressing mtq2－Syx (g) and Venus－VAMP2, which were transfected into CA3

neurons using an AAV1, and of dendritic spines expressing mCherry (h) expressed by gene gun (scale bar, 1 μm). These images were simultaneously acquired with the same excitation laser at 900 nm. (i) The overlap of a bouton (g) and spine (h) in both the xy plane (upper panel) and xz plane along the yellow line (lower panel). (j) A lifetime image of mtq2 obtained from the image (g), which shows a high FRET region at the edge of the axonal bouton facing the spine in both xy and xz images. (k) A fluorescence image of Venus－VAMP2 obtained from the same area at 980nm, where the precise location of Venus－VAMP2 relative to the dendrite was aligned by simultaneous imaging of Venus－VAMP2 and mCherry. (l) The fluorescence profiles along the yellow line in i for mtq2－Syx, Venus－VAMP2, mCherry and A1-A1axon fractions of mtq lifetime images. The cyan-shaded region represents the axonal area where the fluorescent intensity of mtq－Syx was 50 % of the peak value. (m) The correlation between spine volume (V_H) and A1bouton-A1axon. Spearman's rank correlation coefficients were r = 0.59 (P = 0.008, n = 19). (n) The correlation between spine volume (V_H) and the peak A1bouton value at the point facing the spine (A1s-A1axon, n). In addition to the data points in (m), I intentionally sampled more spines from larger spines. Spearman's rank correlations was 0.45 (P = 0.0095, n = 32, the red dashed line) for spines with volumes $<$ 0.2 μm^2, while -0.067 (P = 0.86, n = 18, the blue horizontal dashed line) for spines with volume $>$ 0.2 μm^2. The average A1s–A1axon values for spines with volumes $>$ 0.25 μm^2 was 27.7 ± 2.1 % (n = 16).

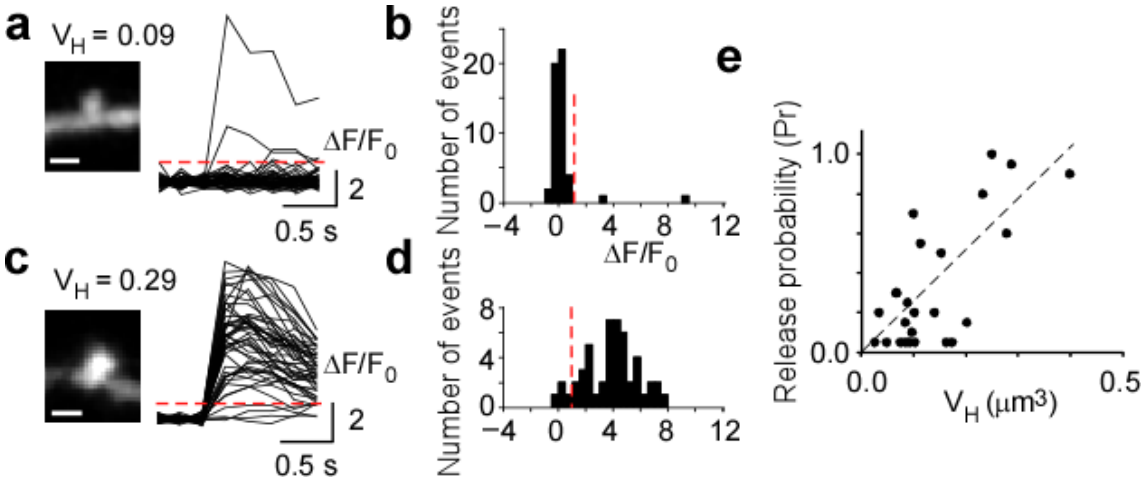

Figure 19 | Ca^{2+} transients in dendritic spines of CA1 pyramidal neurons evoked by electrical stimulation of presynaptic fibers in hippocampal slice cultures.
(a,c) Images of spines (single Z-section) from which Ca^{2+} imaging was performed with GCaMP6s during repetitive presynaptic stimulation, as indicated in the right panels (scale bars, 1 μm). (b,d) Amplitude histograms of evoked Ca^{2+} responses. The red lines indicate the threshold Ca^{2+} responses for successful release events, which are defined as 100 % increases in GCaMP signals above three times the standard deviation of the baseline noise. (e) Probability of success rate plotted against spine volume (P = 0.0062 using Spearman's rank correlation coefficient; r = 0.73; n = 25).

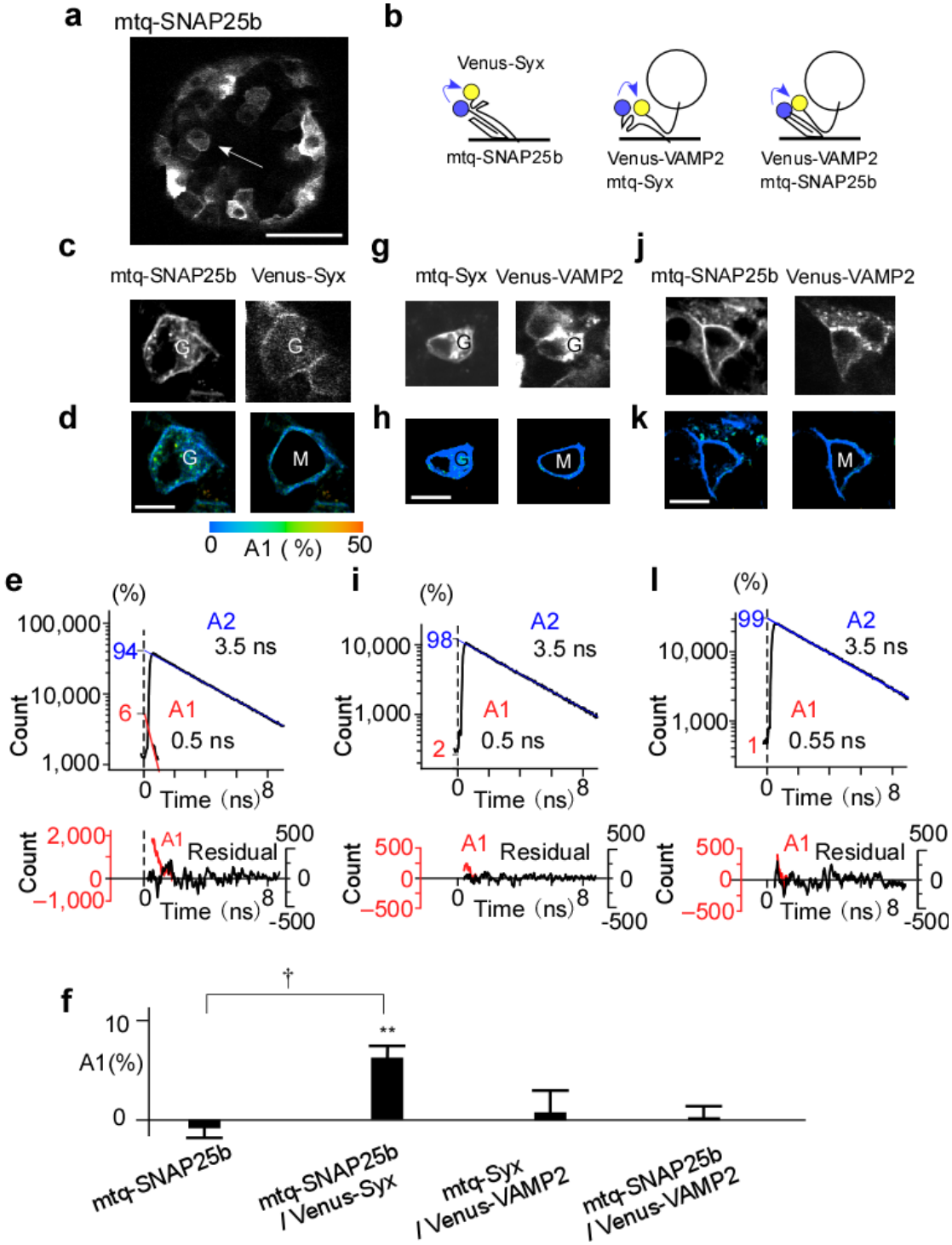

Figure 20 | FRET/2pFLIM with SNARE probes in the β cells in the pancreatic islets of Langerhans.

(a) A fluorescence image of islets transfected with mtq－SNAP25 by lentivirus (scale bar, 50 μm). The arrow indicates the typical cells investigated. (b) Schematic drawings of three FRET probes. (c,d,g,h,j,k) Fluorescence and A1 fraction images of mtq－SNAP25/Venus－Syx (c,d), mtq－Syx/Venus－VAMP2 (g,h) or mtq－SNAP25

and Venus－VAMP2 (j,k) (scale bars, 5 μm). ‘G’ denotes the Golgi apparatus, and ‘M’ in the right panels of images (d,h,k) denotes the masked cytosolic regions. (e,i,l) Lifetime decay curves of the plasma membranes of β cells transfected with mtq－SNAP25/Venus－Syx (b, e), mtq－Syx/Venus－VAMP2 (b, i), and mtq－SNAP25 and Venus－VAMP2 (b, l), which were obtained from 12, 12 and 11 cells, respectively. (f) The average A1 fractions of the lifetime decay of β cell plasma membrane transfected with four different probes indicated. The A1 fractions of mtq－SNAP25 are -0.8 ± 1.1 % (10 cells; $P = 0.14$), those mtq－SNAP25/Venus－Syx are 5.3 ± 1 % (22 cells; $^{**}P < 0.01$), those of mtq－Syx/Venus－VAMP2 are 0.8 ± 2.3 % (15 cells; $P = 0.82$) and those of mtq－SNAP25/Venus－VAMP2 are 0.04 ± 1.4 % (21 cells; $P = 0.89$) at the endogenous expression levels of Venus－Syx and Venus－VAMP2 (Fig. 21d,f ;see Fig.22), respectively. The *P* values were obtained using the Wilcoxon signed-rank test. The four groups were significant in analysis using the Kruskal–Wallis test with $P < 0.007$. Steel’s test versus mtq－SNAP25 yielded $P = 0.014$ for mtq－SNAP25/Venus－Syx, $P = 0.92$ for mtq－Syx/Venus－VAMP2 and $P = 0.74$ for mtq－SNAP25/Venus－VAMP2.

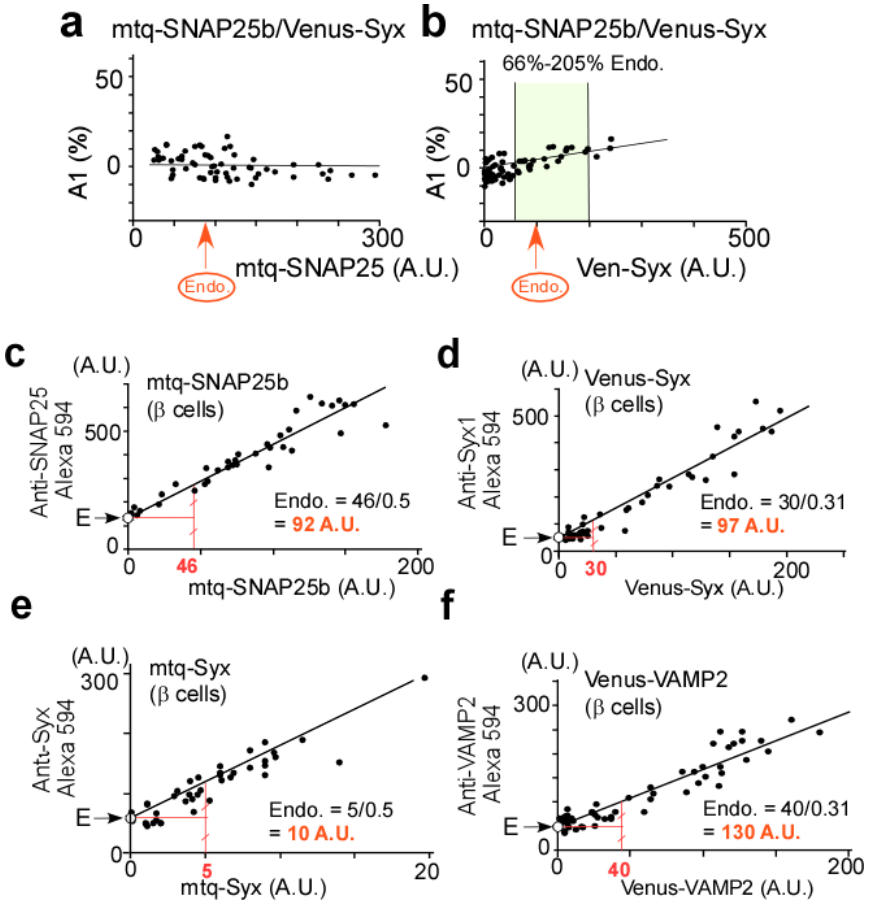

Figure 21 | The Dependence of the A1 Values on the Expression Levels of the Acceptors in β cells in the Pancreatic Islets.

The A1 values for mtq－SNAP25/ Venus－Syx (a,b), The A1 values are estimated from the data using the expression levels of the donor indicated by green shaded areas: 66 %–205 % (b, 114 ± 9 A.U., n = 22). The solid lines are horizontal in (a), and through the origin with the least square fits of the data (b). The correlation coefficients were −0.1 for 68 islet cells, respectively, and the *P* value was 0.001 in (a), using Spearman's rank correlation coefficient. In contrast, the A1 values were more correlated with acceptor expression, particularly in (b). The correlation coefficient was 0.74 for 68 islet cells, and the *P* value was 0.0001 for (b). mtq－SNAP25/Venus－Syx (c,d) and mtq－Syx/Venus－VAMP2 (e,f) plotted against the expression levels of three SNAREs measured by fluorescence intensity of each probe in the region of interest encompassing the plasma membrane in arbitrary unit. The endogenous expression levels of each SNARE protein, 92 A.U. for SNAP25 (mtq), 97 A.U. for Syx (Venus), 10 A.U. for Syx (mtq) and 130 A.U. for VAMP2 (Venus). (c—f)Fluorescence intensities of β cell plasma membrane stained with anti-SNARE antibodies are plotted against the fluorescence intensity of the same proteins labelled with mtq or Venus in β cells in the islets of Langerhans (n = 35, 44, 37, 55).

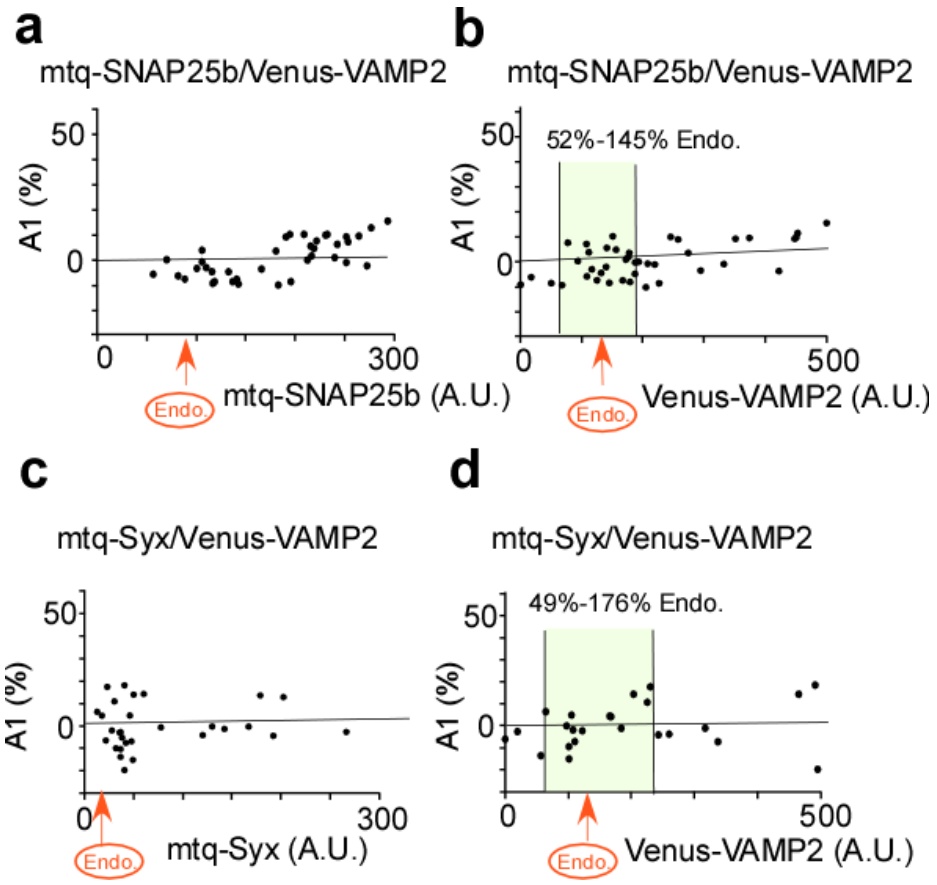

Figure 22 | The Dependence of the A1 Values on the Expression Levels of the Acceptors in β cells in the Pancreatic Islets.

The A1 values for mtq－SNAP25/Venus－VAMP2 (a,b) and mtq－Syx/Venus－VAMP2 (c,d) plotted against the expression levels of three SNAREs measured by fluorescence intensity of each probe in the region of interest encompassing the plasma membrane in arbitrary unit. The A1 values are estimated from the data using the expression levels of the acceptor indicated by green shaded areas: 52–145 % (f, 138 ± 8A.U., n = 21) and 49 %–176 % (d, 139 ± 15 A.U., n = 15) . The solid lines are horizontal in (a, c), and through the origin with the least square fits of the data (b, d). The correlation coefficients were 0.75 and 0.15 for 39 and 29 islet cells, respectively, and the *P* values were 0.0001 and 0.75 in (a) and (c), respectively, using Spearman's rank correlation coefficient. In contrast, the A1 values were more correlated with acceptor expression, particularly in (b). The correlation coefficients were 0.5 and 0.21 for 39 and 29 islet cells, respectively, and the *P* values were 0.0002 and 0.28 for (b) and (d) , respectively.

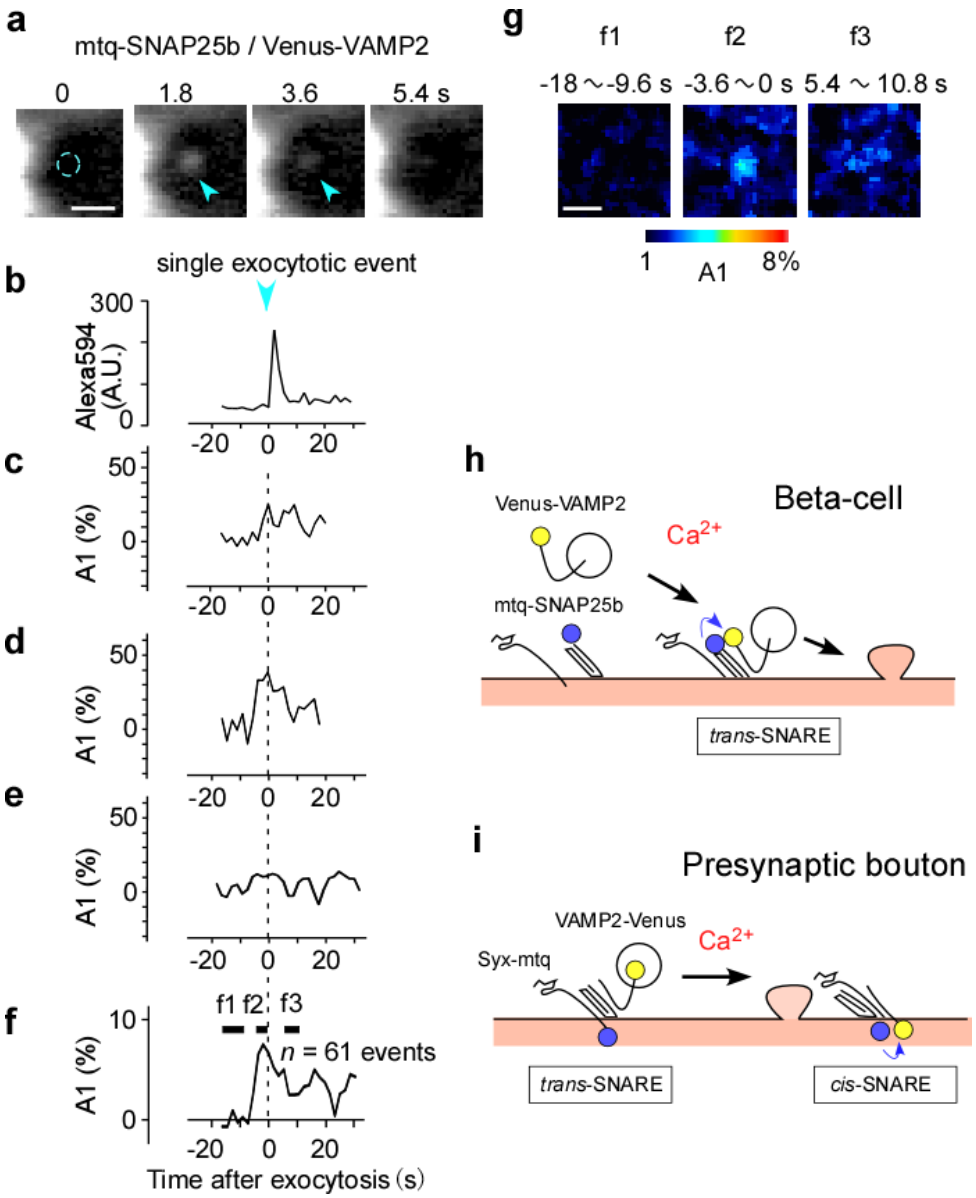

Figure 23 | Increases in FRET signals between SNARE probes by individual exocytosis of insulin vesicles.

(a) Fluorescence images of a pancreatic islet immersed in an Alexa594 solution, where arrowheads indicate an individual exocytotic event (scale bar, 1 μm). The islet was transfected with mtq－SNAP25 and Venus－VAMP2 using a lentivirus, and stimulated with a high-glucose (16 mM) solution. (b) Increases in Alexa594 fluorescence by exocytosis of a single insulin vesicle. (c－e) Increases in the binding fraction of mtq－SNAP25 and Venus－VAMP2 during individual exocytotic events. (f) Average time course of the binding fraction from 61 exocytotic events that were aligned to the onset of the Alexa594 signal (b). (g) A1 images before (f1 and f2) and after exocytosis (f3) (scale bar, 1 μm). (h,i) Schematic illustration of the formation of SNARE complexes and exocytosis in β cells (h) and presynaptic bouton (i).

Table 1

Preparations	Methods	*trans*-SNARE fractions
Dissociated culture	"Subtraction Method"	Mean ± SEM
	Syx/VAMP2 in axons	0.9 % ± 2.2 %
	Syx/VAMP2 in boutons	9.4 % ± 3.6 %
	"Gradient Method" in boutons	
	Syx/VAMP2	11.7 % ± 3.0 %
	SNAP25/VAMP2	14.0 % ± 2.5 %
	SNAP25/VAMP2 in KO mice	11.3 % ± 1.7 %
	SNAP25/Syx	13.3 % ± 3.4 %
	Syx/VAMP2 in AZ	24.2 % ± 2.7 %
Slice culture	"Gradient Method" in boutons	
	Syx/VAMP2	11.9 % ± 10.2 %
	Syx/VAMP2 in AZ	27.7 % ± 2.1 %
Pancreatic islet β cells	Total SNARE complexes in the plasma membrane	
	Syx/VAMP2	0.8 % ± 2.3 %
	SNAP25/VAMP2	0.04 % ± 1.4 %

Table 1｜Estimated fractions of *trans*-SNARE complexes in Syx or SNAP25.
Three different preparations, cortical neurons in dissociated culture, hippocampal pyramidal neurons in slice cultures and β cells in the islets of Langerhans. al neurons n method" utilized the FRET values estimated from the total SNARE assembly minus *cis*-SNARE assembly using Syx/VAMP2 (Fig. 3,9 and 11). "Gradient method" can be applied to all three pairs of SNAREs, and the fractions in the axons were subtracted from those in the boutons (Fig. 9—14). *Trans*-SNARE in the active zone was estimated using the peak A1 values in dissociated culture (Fig. 8d), and those of presynaptic boutons facing the spine with volume larger than 0.25 μm^3 (Fig. 18n). The total binary SNARE complexes were estimated in the plasma membranes of β cells (Fig. 20).